2020

Investigating the Numerical Stability of Using an Impedance Boundary Condition to Model Broadband Noise Scattering With Acoustic Liners

Michelle E. Rodio

Fang Q. Hu
Old Dominion University, fhu@odu.edu

Douglas M. Nark

Original Publication Citation

Rodio, M. E., Hu, F. Q., & Nark, D. M. (2020). Investigating the numerical stability of using an impedance boundary condition to model broadband noise scattering with acoustic liners. AIAA Aviation 2020 Forum, Virtual, June 15-19, 2020. https://doi.org/10.2514/6.2020-2547

AIAA AVIATION Forum
June 15-19, 2020, VIRTUAL EVENT
AIAA AVIATION 2020 FORUM

10.2514/6.2020-2547

Investigating the Numerical Stability of Using an Impedance Boundary Condition to Model Broadband Noise Scattering With Acoustic Liners

Michelle E. Rodio*
Information Technology Infrastructure Branch, NASA Langley Research Center, Hampton, VA 23681, USA

Fang Q. Hu†
Department of Mathematics and Statistics, Old Dominion University, Norfolk, VA 23529, USA

Douglas M. Nark‡
Structural Acoustics Branch, NASA Langley Research Center, Hampton, VA 23681, USA

Reducing aircraft noise is a major objective in the field of computational aeroacoustics. When designing next generation quiet aircraft, it is important to be able to accurately and efficiently predict the acoustic scattering by an aircraft body from a given noise source. Acoustic liners are an effective tool for achieving aircraft noise reduction and are characterized by a frequency-dependent impedance value. Converted into the time-domain using Fourier transforms, an impedance boundary condition can be used to simulate the acoustic wave scattering by geometric bodies treated with acoustic liners. A *Broadband Impedance Model* will be discussed in which the liner impedance is specified along a wide range of frequencies. The liner impedance boundary condition will be derived and coupled with a time-domain boundary integral equation to model acoustic scattering by a flat plate consisting of both un-lined and lined surfaces. The scattering solution will be obtained iteratively using both spatial and temporal basis functions and the stability will be demonstrated through eigenvalue analysis. Stability will be assessed for its dependence on time step, spatial discretization, as well as temporal basis function order. Both second- and third-order backward difference Lagrange temporal basis functions are considered.

Nomenclature

Abbreviations

BD2	Second-Order Backward Difference Scheme
BD3	Third-Order Backward Difference Scheme
BEM	Boundary Element Method
BIE	Boundary Integral Equation
IBC	Impedance Boundary Condition
MOT	March-On-in-Time
TD-BIE	Time-Domain Boundary Integral Equation

Greek Letters

α	Variable Used in the Green's Function Solution, along with: β
α_ℓ	Parameter of *Broadband Impedance Model*, along with: β_ℓ, γ_ℓ
Δt	Numerical Time Step

*AIAA Student Member, michelle.e.rodio@nasa.gov
†Professor and AIAA Associate Fellow
‡Senior Research Scientist and AIAA Associate Fellow

δ	Tolerance of Matrix Power Iteration Method
δ_{ij}	Kronecker Delta Function
λ	Eigenvalue
ρ_0	Average Fluid Density
ϕ_j	Surface Element Basis Function at Node j
ψ_k	Temporal Basis Functions at Time Step Increment k
ω	Frequency Variable

Roman Letters

$\boldsymbol{A}$	Matrix Used for the March-On-in-Time Scheme
A_ℓ	Parameter of *Broadband Impedance Model*, along with: B_ℓ, C_ℓ, h_0, J_1, J_2
A_{INT}	Simplification Used for Burton-Miller Analysis, along with: B_{INT}, C_{INT}
a, b	Stability Condition Parameters Used for Burton-Miller
$\boldsymbol{B}, \boldsymbol{C}$	Matrices Used for Burton-Miller Reformulation
c	Speed of Sound
$\boldsymbol{D}$	Matrix Used for Impedance Boundary Condition, along with: $\boldsymbol{E}$, $\boldsymbol{G}$, $\mathcal{J}$, $\mathcal{K}$, $\mathcal{L}$, $\mathcal{M}$, $\mathcal{N}$, $\boldsymbol{Q}$
E_j	Element on Scattering Body
$\boldsymbol{e}$	Eigenvector
$F(\omega)$	Fourier Transform
G_0	Variable Used in the Green's Function Solution, along with: $\overline{R}$
$\tilde{G}$	Free-Space Adjoint Green's Function
$\boldsymbol{I}$	Identity Matrix
i	Imaginary Unit where $i^2 = -1$
J, K	Variable Used to Denote Finite Number of Time Steps
$\boldsymbol{M}$	Mach Number where $\boldsymbol{M} = \boldsymbol{U}/c$
M_n	Mach Number of Mean Flow Normal to the Scatterer
$\boldsymbol{M_T}$	Tangential Component of Mach Number $\boldsymbol{M}$
N_e, N_t	Total Number of Surface Elements, Time Steps
N_x, N_y, N_z	Surface Discretization Along the x-, y-, and z-Directions
$\boldsymbol{n}$	Unit Normal Vector Pointing Inward to the Scattering Body
$\overline{\boldsymbol{n}}, \tilde{\boldsymbol{n}}$	Modified Normal Derivative, Combined Normal Derivative
$p(\boldsymbol{r}, \omega)$	Acoustic Pressure in the Frequency-Domain
$p(\boldsymbol{r}, t)$	Acoustic Pressure in the Time-Domain
$\boldsymbol{p}_j^{(0,1,2)}$	Solution for the Discretized System of Partial Differential Equations
$q(\boldsymbol{r}, t)$	Known Acoustic Source in the Time-Domain
$\boldsymbol{r}$	Arbitrary Point in Three-Dimensional Space where $\boldsymbol{r} = \boldsymbol{r}(x, y, z)$
$\boldsymbol{r}_s, \boldsymbol{r}'_s$	Arbitrary Point, Observer Point on the Scattering Body Surface
r_j	Collocation Point
S, S_0, S_l	Acoustic Scattering Surface for Rigid (Un-lined), Soft (Lined) Bodies where $S = S_0 \cup S_l$
t	Time Variable
t_k	Time at Time Step Increment k
t'_R	Retarded Time
$\boldsymbol{U}$	Mean Flow Velocity Vector
u_j^k, v_j^k	Numerical Solution of p, $\partial p/\partial n$ on the j-th Node at Time t_k
$\boldsymbol{u^n}, \boldsymbol{v^n}$	Rigid, Soft Body Solution for the Discretized System of Equations
V	Volume Exterior of the Scattering Surface
$\boldsymbol{v}$	Acoustic Velocity Vector
$v(\boldsymbol{r_s}, \omega)$	Volumetric Flow of the Acoustic Wave where $v(\boldsymbol{r_s}, \omega) = \boldsymbol{v} \cdot \boldsymbol{n}$
$\boldsymbol{w^n}$	Solution for the Coupled March-On-in-Time Scheme
$Z(\omega)$	Surface Impedance in Frequency-Domain
$\boldsymbol{0}$	Zero Matrix

I. Introduction

Reducing aircraft noise is a major objective in the field of computational aeroacoustics. When designing next generation quiet and environmentally friendly aircraft, it is important to be able to accurately and efficiently predict the acoustic scattering by an aircraft body from a given noise source [1, 2]. Acoustic scattering problems can be modeled by reformulating the convective wave equation as a boundary integral equation (BIE) and solved iteratively using boundary element methods (BEMs) [3–11]. BEMs are beneficial in that they effectively handle singular and infinite fields, ultimately saving computing memory and maintaining high computational efficiency [1, 3, 12, 13].

Methods for deriving an integral equation for the prediction of acoustic scattering have been studied extensively in both the frequency- and time-domains [8, 14–24]. Frequency-domain solvers are the most used and researched within literature; they have a reduced computational cost, allow for modeling time-harmonic fields at a single frequency, eliminate the growth of Kelvin-Helmholtz instabilities caused by velocity shear of two interacting fluids, and allow for an impedance boundary condition (IBC) to be imposed more naturally. Despite these benefits, there are several distinct advantages to using a time-domain solver [1, 25]. Time-domain solvers allow for the simulation and study of broadband sources and time-dependent transient signals, whereas studying broadband sources in the frequency-domain carry a high computational cost. Time-domain solvers also allow for the scattering solution at all frequencies to be obtained within a single computation and avoid needing to invert a large dense linear system as is required in the frequency-domain. Moreover, a time-domain solution is more naturally coupled with a nonlinear computational fluid dynamics simulation of noise sources.

Time-domain BIEs (TD-BIEs) have an intrinsic numerical instability [3, 4, 26–33] due to the existence of non-unique solutions in the interior domain at resonant modes near the frequency of interest. These non-unique solutions yield an ill-conditioned matrix in the time-domain. Appearing over long run times as exponentially growing oscillations, the numerical instability can be eliminated using a Burton-Miller-type reformulation of the TD-BIE. This method, first introduced in 1971 [34], derives a supplementary integral equation resulting in a unique solution for the exterior problem. The Burton-Miller approach has been studied extensively for eliminating numerical instability [1, 3, 4, 35–39]. This method is computationally expensive to implement and in recent years, numerical techniques for modeling radiative scattering using Burton-Miller-type TD-BIEs have been under development [1, 36–38]. It has been shown not only that stability can be achieved but also that both cost and time can be reduced using fast algorithms and high performance computing.

The objective of this study is to investigate the feasibility and stability for modeling acoustic wave scattering using a Burton-Miller-type TD-BIE with an IBC applied on the scattering surface. Acoustic scattering problems are considered for geometric bodies consisting of both rigid and soft surfaces, the solutions of which are estimated using zeroth-order spatial and either second- or third-order Lagrange temporal basis functions and solved iteratively with BEMs using a March-On-in-Time (MOT) scheme. Herein, soft surfaces are defined to be surfaces in which an acoustic liner is applied. Typically composed of an array of Helmholtz resonators arranged in a honeycomb structure for support and covered with a perforate face-sheet, acoustic liners are used for dissipating the incident acoustic wave and are very effective at absorbing sound [25, 40–45]. Liners can used for suppressing jet engine noise by inlet and exhaust ducts [46], *e.g.*, and work by "inducing vortex shedding at the mouths of resonators" [47].

Impedance, herein denoted by $Z(\omega)$, is a complex-valued quantity such that $\mathrm{Re}(Z)$ is given to be the acoustic resistance and $\mathrm{Im}(Z)$ is given to be the acoustic reactance [25, 42, 43]. Transformed into the time-domain using Fourier transforms, an IBC may be coupled with a TD-BIE to model acoustic wave scattering by soft surfaces. Acoustic liners are characterized by a frequency-dependent impedance value and, when converted into the time-domain, yield a suitable IBC for acoustically treated surfaces.

Since simulation of TD-BIEs without Burton-Miller-type reformulation is prone to numerical instabilities, it is necessary to study the integral equation reformulation to ensure stability of the system once coupled with an IBC. In literature, stability analysis has proven convolution quadrature methods second-order convergent for basis functions constant in space and linear in time [48], but no theoretical proof has yet been provided for other methods. Eigenvalue analysis is the current standard for studying the stability of TD-BIEs [29, 49, 50]. Though eigenvalue analysis alone is not sufficient for proving stability, it is necessary that the numerical scheme has maximum eigenvalues no greater than unity.

In previous work [2, 51], the authors studied the numerical stability of coupling an IBC with a Burton-Miller-type TD-BIE to model radiative scattering by an acoustically treated flat plate. Two numerical models were considered for representing the acoustic liner: the *Extended Helmholtz Resonator Model* [42] and the *Three-Parameter Impedance Model* [47]. In each model, the acoustic liner impedance is specified at a single frequency, educed from experimental measurements. In the studies, eigenvalue analysis was presented and the authors demonstrated that numerical stability

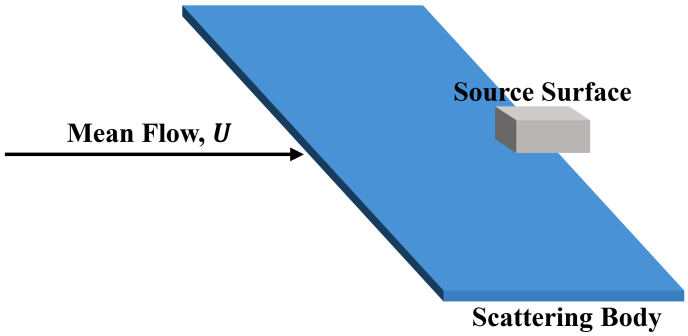

Fig. 1 Schematic diagram illustrating the relationship between the mean flow, the surface of the scattering body, and the surface of the acoustic source.

can be achieved for each model.

Though the *Helmholtz* and *Three-Parameter* models were each shown to be stable [2, 51], they are not ideal models for use in the time-domain considering they are strictly limited a single frequency. One of the key advantages of using time-domain solvers over frequency-domain solvers is the ability to study and simulate broadband sources. In [41], Li, Li, and Tam developed a *Broadband Impedance Model* to represent liner impedance at a wide range of frequencies. The model was derived from the multipole impedance model in [44] and was further studied in the works of Dragna *et. al.* [52] and Troian *et. al.* [53]. The *Broadband* model is a physical model satisfying the requirements of causality, reality, and passivity [41]. The model is derived using recursive combination methods combined with first-order partial differential equations and is effective when used with high-order numerical schemes. Following previous work [2, 51], the authors have now studied the *Broadband Impedance Model* allowing for the investigation of multiple frequencies simultaneously. Stability results will be discussed in subsequent sections.

The outline of this paper is as follows. In Section II, a derivation is provided for the Burton-Miller-type TD-BIE. All derivations follow the cited references as they evolved over time, for completeness. In Section III, the time-domain broadband IBC is derived and discussed. The methodology for conducting the eigenvalue study is presented with all stability results given in Section IV. Concluding remarks are provided in Section V.

II. Burton-Miller-Type Time-Domain Boundary Integral Equation

Acoustic waves are assumed to be disturbances of small amplitudes. With a uniform mean flow, acoustic disturbances are governed by the linear convective wave equation [1, 19–22]. Consider the linear convective wave equation with mean flow $\boldsymbol{U}$:

$$\left(\frac{\partial}{\partial t} + \boldsymbol{U}\cdot\nabla\right)^2 p\left(\boldsymbol{r},t\right) - c^2\nabla^2 p\left(\boldsymbol{r},t\right) = q\left(\boldsymbol{r},t\right) \tag{1}$$

and homogeneous initial conditions:

$$p(\boldsymbol{r},0) = \frac{\partial p}{\partial t}(\boldsymbol{r},0) = 0,\ t = 0 \tag{2}$$

where $\boldsymbol{r}$ is an arbitrary point in three-dimensional space, $p(\boldsymbol{r},t)$ is the acoustic pressure, $q(\boldsymbol{r},t)$ is the known acoustic source, and c is the speed of sound. The solution of (1) with initial conditions (2) is dependent on the applied boundary conditions on the surface or collection of surfaces, S, for the scattering problem as illustrated in Figure 1.

As demonstrated by the authors in [1, 37, 38, 51, 54], the convective wave equation (1) and initial conditions (2), along with suitable boundary conditions, can be reformulated into a TD-BIE first by introducing a free-space adjoint Green's function $\tilde{G}(\boldsymbol{r},t;\boldsymbol{r'},t')$ and then by taking the limit as an arbitrary point $\boldsymbol{r'}$ approaches a boundary point $\boldsymbol{r}'_s$. The Green's function is defined as:

$$\tilde{G}(\boldsymbol{r},t;\boldsymbol{r'},t') = \frac{G_0}{4\pi c^2}\,\delta\left(t'-t+\boldsymbol{\beta}\cdot(\boldsymbol{r'}-\boldsymbol{r}) - \frac{\overline{R}}{c\alpha^2}\right) \tag{3}$$

where

$$\overline{R}(\boldsymbol{r},\boldsymbol{r'}) = \sqrt{\left|\boldsymbol{M}\cdot(\boldsymbol{r}-\boldsymbol{r'})\right|^2 + \alpha^2\left|\boldsymbol{r}-\boldsymbol{r'}\right|^2},\ G_0 = \frac{1}{\overline{R}(\boldsymbol{r},\boldsymbol{r'})} \tag{4}$$

in which

$$\boldsymbol{M} = \frac{\boldsymbol{U}}{c},\ \alpha = \sqrt{1 - M^2},\ \text{and}\ \boldsymbol{\beta} = \frac{\boldsymbol{M}}{1 - M^2} \tag{5}$$

for Mach number $\boldsymbol{M}$. Assuming that $\boldsymbol{r}'_s$ is a smooth boundary collocation point, the resulting TD-BIE is given by [51]:

$$Q(\boldsymbol{r}'_s, t') = 2\pi p(\boldsymbol{r}'_s, t') - \int_S \left[G_0 \frac{\partial p}{\partial \tilde{n}}(\boldsymbol{r}_s, t'_R) - \frac{\partial G_0}{\partial \overline{n}} \left(p(\boldsymbol{r}_s, t'_R) + \frac{\overline{R}}{c\alpha^2} \frac{\partial p}{\partial t}(\boldsymbol{r}_s, t'_R) \right) \right] d\boldsymbol{r}_s \tag{6}$$

where

$$Q(\boldsymbol{r}'_s, t') = \frac{1}{c^2} \int_V G_0 q(\boldsymbol{r}_s, t'_R) d\boldsymbol{r}_s$$

such that V denotes the region of acoustic surfaces and S denotes the scattering surface. Further, t'_R denotes the retarded time at an arbitrary point and, along with G_0, $\overline{R}$, and α, is defined by parameters of the Green's function (3). Moreover, $\partial/\partial\overline{n} = \partial/\partial n - M_n(\boldsymbol{M} \cdot \nabla) = (\boldsymbol{n} - M_n\boldsymbol{M}) \cdot \nabla$ denotes a *modified normal derivative* and $\partial/\partial\tilde{n} = \partial/\partial\overline{n} - (M_n/c)\,\partial/\partial t$ denotes a *combined normal derivative* assuming an inward normal vector $\boldsymbol{n}$ on the scattering body. Here, $M_n = \boldsymbol{M} \cdot \boldsymbol{n}$.

Equation (6) is the Kirchhoff integral representation of the acoustic field for a source in a general mean flow. The solution of (6), $p(\boldsymbol{r}'_s, t')$, is related to the direct contribution of the source noise q as well as the surface contribution involving the retarded time values of p and their normal derivatives. When the pressure p and its derivatives are calculated on the surface S, (6) predicts the pressure at an arbitrary observer point $\boldsymbol{r}'_s$ exterior to or on the boundary of the surface S. In this work, it is assumed that the scattering surface is decomposed into rigid and soft surfaces, S_0 and S_I, respectively, such that $S = S_0 \cup S_I$. On rigid surfaces, a Zero Energy Flux boundary condition [1] is imposed: $\partial p/\partial\tilde{n} = 0$. On soft surfaces, an IBC is imposed, herein represented by the *Broadband Impedance Model* and further discussed in Section III.

TD-BIEs are known to have an intrinsic numerical instability due to resonant frequencies resulting from non-trivial solutions in the interior domain. Using a Burton-Miller type reformulation of (6), resonant frequencies can be eliminated and stability achieved. As demonstrated in [1, 37, 38, 51, 54], the reformulation results by taking the derivative of (6) in the form of:

$$a\frac{\partial}{\partial t'} + bc\frac{\partial}{\partial \tilde{n}'}$$

where a and b are arbitrary parameters that must satisfy the stability condition: $a/b < 0$. Applying the Zero Energy Flux boundary condition, the resulting Burton-Miller-type TD-BIE is given by:

$$\begin{aligned} &4\pi a C_s \frac{\partial p}{\partial t'}(\boldsymbol{r}'_s, t') + 4\pi bc C_s \frac{\partial p}{\partial \tilde{n}'}(\boldsymbol{r}'_s, t') + 4\pi bc \frac{\partial C_s}{\partial \tilde{n}'} p(\boldsymbol{r}'_s, t') \\ &\qquad = a\frac{\partial Q}{\partial t'}(\boldsymbol{r}'_s, t') + bc\frac{\partial Q}{\partial \tilde{n}'}(\boldsymbol{r}'_s, t') + a\,(A_{\text{INT}}) + bc\,(B_{\text{INT}}) + \frac{b}{\alpha^2}\,(C_{\text{INT}}) \end{aligned} \tag{7}$$

where

$$\begin{aligned} A_{\text{INT}} = &\int_S G_0 \left(1 - M_n^2\right) \frac{\partial}{\partial t} \left(\frac{\partial p}{\partial n} \left(\boldsymbol{r}_s, t'_R\right) \right) d\boldsymbol{r}_s - \int_S \frac{\partial G_0}{\partial \overline{n}} \left[\frac{\partial p}{\partial t} \left(\boldsymbol{r}_s, t'_R\right) + \frac{\overline{R}}{c\alpha^2} \frac{\partial^2 p}{\partial t^2} \left(\boldsymbol{r}_s, t'_R\right) \right] d\boldsymbol{r}_s \\ &- \int_S M_n G_0 \left[\boldsymbol{M_T} \cdot \nabla \frac{\partial p}{\partial t} \left(\boldsymbol{r}_s, t'_R\right) + \frac{1}{c} \frac{\partial^2 p}{\partial t^2} \left(\boldsymbol{r}_s, t'_R\right) \right] d\boldsymbol{r}_s, \end{aligned}$$

$$\begin{aligned} B_{\text{INT}} = &\int_S \left(1 - M_n^2\right) \left[\frac{\partial G_0}{\partial \tilde{n}'} \frac{\partial p}{\partial n} \left(\boldsymbol{r}_s, t'_R\right) + G_0 \frac{\partial}{\partial \tilde{n}'} \left(\frac{\partial p}{\partial n} \right) \right] \left(\boldsymbol{r}_s, t'_R\right) d\boldsymbol{r}_s \\ &- \int_S \frac{\partial^2 G_0}{\partial \overline{n} \partial \tilde{n}'} \left[p\left(\boldsymbol{r}_s, t'_R\right) + \frac{\overline{R}}{c\alpha^2} \frac{\partial p}{\partial t} \left(\boldsymbol{r}_s, t'_R\right) \right] d\boldsymbol{r}_s \\ &- \int_S M_n \frac{\partial G_0}{\partial \tilde{n}'} \left[\boldsymbol{M_T} \cdot \nabla p \left(\boldsymbol{r}_s, t'_R\right) + \frac{1}{c} \frac{\partial p}{\partial t} \left(\boldsymbol{r}_s, t'_R\right) \right] d\boldsymbol{r}_s, \end{aligned}$$

$$C_{\text{INT}} = -\int_S \frac{\partial G_0}{\partial \overline{n}} \left[\left(\boldsymbol{M} \cdot \overline{\boldsymbol{n}}' \right) \frac{\partial p}{\partial t} \left(\boldsymbol{r}_s, t'_R \right) + \frac{\overline{R}}{c\alpha^2} \left(\boldsymbol{M} \cdot \overline{\boldsymbol{n}}' - \frac{\partial \overline{R}}{\partial \tilde{n}'} \right) \frac{\partial^2 p}{\partial t^2} \left(\boldsymbol{r}_s, t'_R \right) \right] d\boldsymbol{r}_s$$
$$- \int_S M_n G_0 \left(\boldsymbol{M} \cdot \overline{\boldsymbol{n}}' - \frac{\partial \overline{R}}{\partial \tilde{n}'} \right) \left[\boldsymbol{M_T} \cdot \nabla \frac{\partial p}{\partial t} \left(\boldsymbol{r}_s, t'_R \right) + \frac{1}{c} \frac{\partial^2 p}{\partial t^2} \left(\boldsymbol{r}_s, t'_R \right) \right] d\boldsymbol{r}_s,$$

and where $C_s = 0$ when $\boldsymbol{r}'_s$ is on the interior of S, $C_s = 1$ when $\boldsymbol{r}'_s$ is on the exterior of S, and $C_s = 1/2$ when $\boldsymbol{r}'_s$ is a smooth point on the boundary of S. In (7), $M_n = \boldsymbol{M} \cdot \boldsymbol{n}$ is the Mach number of mean flow normal to the body surface such that $\boldsymbol{n}$ points inward to the body, $\overline{\boldsymbol{n}}$ is the *modified normal derivative*, $\tilde{\boldsymbol{n}}$ is the *combined normal derivative*, and $\boldsymbol{M_T}$ is the tangential component of $\boldsymbol{M}$. For the current study, the simple case of $\boldsymbol{M} = \boldsymbol{0}$ is considered. Under this condition, $\partial p/\partial \tilde{n}$ is reduced to $\partial p/\partial n$.

The stable Burton-Miller-type reformulation (7) of the time-domain boundary integral equation (6) is discretized using collocation methods as detailed in [2, 36]. The surface S is divided into a set of N_e boundary elements $\{E_j, j = 1, \ldots, N_e\}$ where the collocation point $\boldsymbol{r}_j$ is located at the centroid of E_j. The time-domain is divided into N_t uniform time steps where $t_k = k\Delta t$. It is further assumed that the scattering surface S is comprised of both rigid and soft surfaces, denoted herein by S_0 and S_l, respectively, such that $S = S_0 \cup S_l$.

The solution to (7), $p(\boldsymbol{r}'_s, t')$, is obtained by approximating terms involving $p(\boldsymbol{r}_s, t)$ and $\partial p/\partial n(\boldsymbol{r}_s, t)$ using surface element basis functions $\phi_j(\boldsymbol{r}_s)$ and temporal basis functions $\psi_k(t)$ as follows:

$$p(\boldsymbol{r}_s, t) = \sum_{k=0}^{N_t} \sum_{j=1}^{N_e} u_j^k \phi_j(\boldsymbol{r}_s) \psi_k(t) \tag{8}$$

and

$$\frac{\partial p}{\partial n}(\boldsymbol{r}_s, t) = \sum_{k=0}^{N_t} \sum_{j=1}^{N_e} v_j^k \phi_j(\boldsymbol{r}_s) \psi_k(t). \tag{9}$$

In (8) and (9), u_j^k and v_j^k denote the value of the solution of $p(\boldsymbol{r}_s, t)$ and $\partial p/\partial n(\boldsymbol{r}_s, t)$, respectively, of the j-th node at time t_k. For soft body scattering, the Burton-Miller-type reformulation includes terms involving both $p(\boldsymbol{r}_s, t)$ and $\partial p/\partial n(\boldsymbol{r}_s, t)$ which are approximated using (8) and (9), respectively. For strict rigid body scattering, on the other hand, $v_j^k \equiv 0$ by default, *i.e.*, $\partial p/\partial n(\boldsymbol{r}_s, t) = 0$. The Burton-Miller-type reformulation is then reduced to terms involving $p(\boldsymbol{r}_s, t)$ only, the terms which are then approximated using (8).

Following [36], the spatial basis functions (10) are zeroth-order, *i.e.*, constant over each element E_j, and the integrations are computed by high-order Gauss quadrature on a 6×6 grid:

$$\phi_j(\boldsymbol{r}_s) = \left\{ \begin{array}{ll} 1, & \boldsymbol{r}_s \text{ on element } E_j \text{ that contains node } \boldsymbol{r_j} \\ 0, & \text{other} \end{array} \right\}. \tag{10}$$

For the temporal basis functions

$$\psi_k(t) = \Psi\left(\frac{t - t_k}{\Delta t} \right),$$

both second- and third-order backward difference Lagrange functions are considered as defined by (11) and (12), respectively:

$$\Psi(\tau) = \left\{ \begin{array}{ll} 1 + \frac{3}{2}\tau + \frac{1}{2}\tau^2, & -1 < \tau \le 0 \\ 1 - \tau^2, & 0 < \tau \le 1 \\ 1 - \frac{3}{2}\tau + \frac{1}{2}\tau^2, & 1 < \tau \le 2 \\ 0, & \text{other} \end{array} \right\} \tag{11}$$

and

$$\Psi(\tau) = \left\{ \begin{array}{ll} 1 + \frac{11}{6}\tau + \tau^2 + \frac{1}{6}\tau^3, & -1 < \tau \le 0 \\ 1 + \frac{1}{2}\tau - \tau^2 - \frac{1}{2}\tau^3, & 0 < \tau \le 1 \\ 1 - \frac{1}{2}\tau - \tau^2 + \frac{1}{2}\tau^3, & 1 < \tau \le 2 \\ 1 - \frac{11}{6}\tau + \tau^2 - \frac{1}{6}\tau^3, & 2 < \tau \le 3 \\ 0, & \text{other} \end{array} \right\}. \tag{12}$$

Herein, the second-order temporal functions (11) are denoted as "BD2" and the third-order functions (11) are denoted as "BD3." For BD2, the contribution from any node to the solution at collocation point $\boldsymbol{r}_j$ and time step t_n reduces to a summation of three terms, *i.e.*, the solution at t_n is interpolated using time steps t_{n-2}, t_{n-1}, t_n. For BD3, the solution at collocation point $\boldsymbol{r}_j$ and time step t_n reduces to a summation of four terms.

By evaluating the discretized Burton-Miller-type reformulation at collocation points $\boldsymbol{r}_j$ on elements E_j, $j = 1, \ldots, N_e$ and at time step t_n using basis functions (10), (11), and (12), (7) is cast into the following system of equations:

$$\boldsymbol{B_0 u^n} + \boldsymbol{C_0 v^n} = \boldsymbol{q^n} - \boldsymbol{B_1 u^{n-1}} - \boldsymbol{C_1 v^{n-1}} - \boldsymbol{B_2 u^{n-2}} - \boldsymbol{C_2 v^{n-2}} - \ldots - \boldsymbol{B_J u^{n-J}} - \boldsymbol{C_J v^{n-J}} \tag{13}$$

where $\boldsymbol{u}^k$ and $\boldsymbol{v}^k$ denote the vector that contains all unknowns $\left\{u_j^k,\ j = 1, ..., N_e\right\}$ and $\left\{v_j^k,\ j = 1, ..., N_e\right\}$, respectively, at time level t_k. Due to the limited temporal stencil width of (11) and (12), the $\boldsymbol{B}$ and $\boldsymbol{C}$ matrices are sparse. Additionally, the index J denotes the maximum time history of the solution required for (13) and is dependent on the dimensions of the scattering surface and the mean flow [54]. The non-zero entries for both $\boldsymbol{B}$ and $\boldsymbol{C}$ are given in [51].

Assuming rigid body scattering only, $\boldsymbol{v}^k$ is equivalently zero thereby reducing (13) to:

$$\boldsymbol{B_0 u^n} = \boldsymbol{q^n} - \boldsymbol{B_1 u^{n-1}} - \boldsymbol{B_2 u^{n-2}} - \ldots - \boldsymbol{B_J u^{n-J}},$$

the solution of which is easily obtained through an iterative process. Assuming both rigid and soft body scattering, a second system of equations is needed to couple with (13) for obtaining solutions of both $\boldsymbol{u^k}$ and $\boldsymbol{v^k}$. As demonstrated by the authors in [51] and [2], this system results from applying an IBC as discussed in Section III.

III. Broadband Impedance Boundary Condition and March-On-in-Time Scheme

Acoustic scattering of a sound field from a given noise source is predicted for objects in a stationary medium, *i.e.*, assuming a model with no mean flow $\boldsymbol{U}$. With no mean flow, the acoustic pressure in the frequency-domain $p(\boldsymbol{r_s}, \omega)$ is defined [47, 55, 56] as:

$$p(\boldsymbol{r_s}, \omega) = Z(\omega) v(\boldsymbol{r_s}, \omega) \tag{14}$$

where $v(\boldsymbol{r_s}, \omega) = \boldsymbol{v} \cdot \boldsymbol{n}$ is the volumetric flow of the acoustic wave, $\boldsymbol{v}$ is the acoustic velocity vector, $\boldsymbol{n}$ is the inward normal vector on the scattering body, and $Z(\omega)$ is the surface impedance. In the frequency-domain, v is defined [7] as:

$$v(\boldsymbol{r_s}, \omega) = \frac{1}{\rho_0 (i\omega)} \frac{\partial p}{\partial n}(\boldsymbol{r_s}, \omega) \tag{15}$$

where $\partial p / \partial n(\boldsymbol{r_s}, \omega)$ is the normal derivative of acoustic pressure, ρ_0 is the average fluid density, and i is the imaginary unit ($i^2 = -1$). Given the definitions (14) and (15), the acoustic pressure is related to frequency-domain impedance by:

$$\rho_0 (i\omega) p(\boldsymbol{r_s}, \omega) = \frac{\partial p}{\partial n}(\boldsymbol{r_s}, \omega) Z(\omega). \tag{16}$$

In the *Broadband Impedance Model* [41, 52, 53], the frequency-domain surface impedance is defined to be:

$$Z(\omega) = (-i\omega) h_0 + R_0 + \sum_{\ell=1}^{J_1} \frac{A_\ell}{\gamma_\ell - i\omega} + \frac{1}{2} \sum_{\ell=1}^{J_2} \left[\frac{B_\ell + iC_\ell}{\alpha_\ell + i\beta_\ell - i\omega} + \frac{B_\ell - iC_\ell}{\alpha_\ell - i\beta_\ell - i\omega} \right], \tag{17}$$

where causality, passivity, and stability lead to $h_0, R_0 > 0$, $\gamma_k > 0$ for all $\ell = 1, \ldots, J_1$, and $\alpha_k > 0$ for all $\ell = 1, \ldots, J_2$. The impedance $Z(\omega)$ is non-dimensionalized by $\rho_0 c$ where ρ_0 is the average fluid density and c is the speed of sound. Rearranging (17) yields:

$$Z(\omega) = (-i\omega) h_0 + R_0 + \sum_{\ell=1}^{J_1} A_\ell \left[\frac{1}{\gamma_\ell - i\omega} \right] + \sum_{\ell=1}^{J_2} B_\ell \left[\frac{\alpha_\ell - i\omega}{(\alpha_\ell - i\omega)^2 + \beta_\ell^2} \right] + \sum_{\ell=1}^{J_2} C_\ell \left[\frac{\beta_\ell}{(\alpha_\ell - i\omega)^2 + \beta_\ell^2} \right]. \tag{18}$$

Substituting (18) into (16) yields:

$$\begin{aligned} \rho_0 (i\omega) p(\boldsymbol{r_s}, \omega) = (-i\omega) h_0 \frac{\partial p}{\partial n}(\boldsymbol{r_s}, \omega) + R_0 \frac{\partial p}{\partial n}(\boldsymbol{r_s}, \omega) + \sum_{\ell=1}^{J_1} A_\ell \left[\frac{1}{\gamma_\ell - i\omega} \frac{\partial p}{\partial n}(\boldsymbol{r_s}, \omega) \right] \\ + \sum_{\ell=1}^{J_2} B_\ell \left[\frac{\alpha_\ell - i\omega}{(\alpha_\ell - i\omega)^2 + \beta_\ell^2} \frac{\partial p}{\partial n}(\boldsymbol{r_s}, \omega) \right] + \sum_{\ell=1}^{J_2} C_\ell \left[\frac{\beta_\ell}{(\alpha_\ell - i\omega)^2 + \beta_\ell^2} \frac{\partial p}{\partial n}(\boldsymbol{r_s}, \omega) \right]. \end{aligned} \tag{19}$$

To facilitate the conversion of (18) to the time-domain, the following frequency-domain terms are defined:

$$p_\ell^{(0)}(\boldsymbol{r}_s,\omega) = \frac{1}{\gamma_\ell - i\omega}\frac{\partial p}{\partial n}(\boldsymbol{r}_s,\omega) \text{ for all } \ell = 1,\ldots,J_1, \tag{20}$$

$$p_\ell^{(1)}(\boldsymbol{r}_s,\omega) = \frac{\alpha_\ell - i\omega}{(\alpha_\ell - i\omega)^2 + \beta_\ell^2}\frac{\partial p}{\partial n}(\boldsymbol{r_s},\omega) \text{ for all } \ell = 1,\ldots,J_2, \text{ and} \tag{21}$$

$$p_\ell^{(2)}(\boldsymbol{r}_s,\omega) = \frac{\beta_\ell}{(\alpha_\ell - i\omega)^2 + \beta_\ell^2}\frac{\partial p}{\partial n}(\boldsymbol{r_s},\omega) \text{ for all } \ell = 1,\ldots,J_2. \tag{22}$$

Substituting (20), (21), and (22) into (19) yields:

$$\rho_0(i\omega)p(\boldsymbol{r_s},\omega) = (-i\omega)h_0\frac{\partial p}{\partial n}(\boldsymbol{r_s},\omega) + R_0\frac{\partial p}{\partial n}(\boldsymbol{r_s},\omega) + \sum_{\ell=1}^{J_1} A_\ell p_\ell^{(0)}(\boldsymbol{r}_s,\omega) + \sum_{\ell=1}^{J_2} B_\ell p_\ell^{(1)}(\boldsymbol{r}_s,\omega) + \sum_{\ell=1}^{J_2} C_\ell p_\ell^{(2)}(\boldsymbol{r}_s,\omega). \tag{23}$$

For time-domain analysis, (20) through (23) must be transformed from the frequency-domain to the time-domain using Fourier transforms. Define the Fourier transform $F(\omega)$ as:

$$F(\omega) = \frac{1}{2\pi}\int_{-\infty}^{\infty} f(t)e^{i\omega t}dt. \tag{24}$$

With this definition, the inverse Fourier transform of $(-i\omega)^n F(\omega)$ is equal to $d^n f(t)/dt^n$. Taking the inverse Fourier transform of (23) using (24) yields a time-domain broadband IBC for soft surfaces:

$$0 = \rho_0\frac{\partial p}{\partial t}(\boldsymbol{r_s},t) + h_0\frac{\partial}{\partial t}\left(\frac{\partial p}{\partial n}(\boldsymbol{r_s},t)\right) + R_0\frac{\partial p}{\partial n}(\boldsymbol{r_s},t) + \sum_{\ell=1}^{J_1} A_\ell p_\ell^{(0)}(\boldsymbol{r}_s,t) + \sum_{\ell=1}^{J_2} B_\ell p_\ell^{(1)}(\boldsymbol{r}_s,t) + \sum_{\ell=1}^{J_2} C_\ell p_\ell^{(2)}(\boldsymbol{r}_s,t). \tag{25}$$

Moreover, taking the inverse Fourier transform of (20) using (24) yields the following time-domain partial-differential equation given by (26). For all $\ell = 1,\ldots,J_1$:

$$\frac{\partial p}{\partial n}(\boldsymbol{r_s},t) - \frac{\partial p_\ell^{(0)}}{\partial t}(\boldsymbol{r_s},t) - \gamma_\ell p_\ell^{(0)}(\boldsymbol{r_s},t) = 0. \tag{26}$$

Then, adding $(\alpha_\ell - i\omega)\times p_\ell^{(1)}$ to $\beta_\ell \times p_\ell^{(2)}$ using (21) and (22) and taking the inverse Fourier transform using (24) yields a second time-domain partial-differential equation given by (27). For all $\ell = 1,\ldots,J_2$ yields:

$$\frac{\partial p}{\partial n}(\boldsymbol{r_s},t) - \frac{\partial p_\ell^{(1)}}{\partial t}(\boldsymbol{r}_s,t) - \alpha_\ell p_\ell^{(1)}(\boldsymbol{r}_s,t) - \beta_\ell p_\ell^{(2)}(\boldsymbol{r}_s,t) = 0. \tag{27}$$

Finally, substituting (22) into (21) and taking the inverse Fourier transform using (24) yields a third time-domain partial-differential equation given by (27). For all $\ell = 1,\ldots,J_2$ yields:

$$\beta_\ell p_\ell^{(1)}(\boldsymbol{r}_s,t) - \frac{\partial p_\ell^{(2)}}{\partial t}(\boldsymbol{r}_s,t) - \alpha_\ell p_\ell^{(2)}(\boldsymbol{r}_s,t) = 0. \tag{28}$$

The time-domain broadband IBC (25) and subsequent partial differential equations (26) through (28) are discretized by approximating terms involving $p(\boldsymbol{r}_s,t)$ and $\partial p/\partial n(\boldsymbol{r}_s,t)$ using surface element basis functions $\phi_j(\boldsymbol{r}_s)$ and temporal basis functions $\psi_k(t)$ defined by (10) through (12), and by approximating terms involving $p_\ell^{(m)}(\boldsymbol{r}_s,t)$ by:

$$p_\ell^{(m)}(\boldsymbol{r}_s,t) = \sum_{k=0}^{N_t}\sum_{j=1}^{N_e}\left(p_\ell^{(m)}\right)_j^k \phi_j(\boldsymbol{r}_s)\psi_k(t), m = 0,1,2.$$

Evaluating at collocation points $\boldsymbol{r}_i, i = 1,\ldots,N_e$ and time step t_n yields the following discretized broadband IBC and

subsequent partial differential equations:

$$0 = \sum_{k=0}^{N_t}\sum_{j=1}^{N_e}\delta_{ij}\left[u_j^k\rho_0\psi_k'(t_n) + v_j^k\left(h_0\psi_k'(t_n) + R_0\psi_k(t_n)\right)\right] \tag{29}$$
$$+ \sum_{k=0}^{N_t}\sum_{j=1}^{N_e}\delta_{ij}\left[\sum_{\ell=1}^{J_1}\left(p_\ell^{(0)}\right)_j^k A_\ell\psi_k(t_n) + \sum_{\ell=1}^{J_2}\left(p_\ell^{(1)}\right)_j^k B_\ell\psi_k(t_n) + \sum_{\ell=1}^{J_2}\left(p_\ell^{(2)}\right)_j^k C_\ell\psi_k(t_n)\right]$$

$$0 = \sum_{k=0}^{N_t}\sum_{j=1}^{N_e}\delta_{ij}\left[v_j^k\psi_k(t_n) - \sum_{\ell=1}^{J_1}\left(p_\ell^{(0)}\right)_j^k\left(\psi_k'(t_n) + \gamma_\ell\psi_k(t_n)\right)\right], \tag{30}$$

$$0 = \sum_{k=0}^{N_t}\sum_{j=1}^{N_e}\delta_{ij}\left[v_j^k\psi_k(t_n) - \sum_{\ell=1}^{J_2}\left(p_\ell^{(1)}\right)_j^k\left(\psi_k'(t_n) + \alpha_\ell\psi_k(t_n)\right) - \sum_{\ell=1}^{J_2}\left(p_\ell^{(2)}\right)_j^k\beta_\ell\psi_k(t_n)\right], \text{ and} \tag{31}$$

$$0 = \sum_{k=0}^{N_t}\sum_{j=1}^{N_e}\delta_{ij}\left[\sum_{\ell=1}^{J_2}\left(p_\ell^{(1)}\right)_j^k\beta_\ell\psi_k(t_n) - \sum_{\ell=1}^{J_2}\left(p_\ell^{(2)}\right)_j^k\left(\psi_k'(t_n) + \alpha_\ell\psi_k(t_n)\right)\right]. \tag{32}$$

The series solutions (29) through (32) are equivalent to the results of discretizing (25) through (28) by an implicit backward difference scheme [57].

The following vectors are additionally defined:

$$\boldsymbol{P}_{(0)} = [\boldsymbol{p}_1^{(0)}\boldsymbol{p}_2^{(0)}\cdots\boldsymbol{p}_{J_1}^{(0)}]^T, \boldsymbol{P}_{(1)} = [\boldsymbol{p}_1^{(1)}\boldsymbol{p}_2^{(1)}\cdots\boldsymbol{p}_{J_1}^{(1)}]^T, \text{ and } \boldsymbol{P}_{(2)} = [\boldsymbol{p}_1^{(2)}\boldsymbol{p}_2^{(2)}\cdots\boldsymbol{p}_{J_1}^{(2)}]^T \tag{33}$$

where $\boldsymbol{p}_j^{(0)}, \boldsymbol{p}_j^{(1,2)}$ denote the vectors that contain auxiliary variables from all points where the IBC is applied. Using (33), the discretizations (29) through (32) are then written as the following system of equations with a finite number of K time steps:

$$\begin{aligned}\boldsymbol{D_0u^n} + \boldsymbol{E_0v^n} + \boldsymbol{F_0}\boldsymbol{P}_{(0)}^n + \boldsymbol{G_0}\boldsymbol{P}_{(1)}^n + \boldsymbol{H_0}\boldsymbol{P}_{(2)}^n = \boldsymbol{0} - \boldsymbol{D_1u^{n-1}} - \boldsymbol{E_1v^{n-1}} - \boldsymbol{F_1}\boldsymbol{P}_{(0)}^{n-1} - \boldsymbol{G_1}\boldsymbol{P}_{(1)}^{n-1} - \boldsymbol{H_1}\boldsymbol{P}_{(2)}^{n-1} - \cdots - \\ - \boldsymbol{D_K u^{n-K}} - \boldsymbol{E_K v^{n-K}} - \boldsymbol{F_K}\boldsymbol{P}_{(0)}^{n-K} - \boldsymbol{G_K}\boldsymbol{P}_{(1)}^{n-K} - \boldsymbol{H_K}\boldsymbol{P}_{(2)}^{n-K}\end{aligned} \tag{34}$$

$$\mathcal{J}_0\boldsymbol{v^n} + \mathcal{K}_0\boldsymbol{P}_{(0)}^n = \boldsymbol{0} - \mathcal{J}_1\boldsymbol{v^{n-1}} - \mathcal{K}_1\boldsymbol{P}_{(0)}^{n-1} - \cdots - \mathcal{J}_K\boldsymbol{v^{n-K}} - \mathcal{K}_K\boldsymbol{P}_{(0)}^{n-K} \tag{35}$$

$$\boldsymbol{\mathcal{L}_0v^n} + \boldsymbol{\mathcal{M}_0}\boldsymbol{P}_{(1)}^n + \boldsymbol{\mathcal{N}_0}\boldsymbol{P}_{(2)}^n = \boldsymbol{0} - \boldsymbol{\mathcal{L}_1v^{n-1}} - \boldsymbol{\mathcal{M}_1}\boldsymbol{P}_{(1)}^{n-1} - \boldsymbol{\mathcal{N}_1}\boldsymbol{P}_{(2)}^{n-1} - \cdots - \boldsymbol{\mathcal{L}_K v^{n-K}} - \boldsymbol{\mathcal{M}_K}\boldsymbol{P}_{(1)}^{n-K} - \boldsymbol{\mathcal{N}_K}\boldsymbol{P}_{(2)}^{n-K} \tag{36}$$

$$\boldsymbol{\mathcal{P}_0}\boldsymbol{P}_{(1)}^n + \boldsymbol{\mathcal{Q}_0}\boldsymbol{P}_{(2)}^n = \boldsymbol{0} - \boldsymbol{\mathcal{P}_1}\boldsymbol{P}_{(1)}^{n-1} - \boldsymbol{\mathcal{Q}_1}\boldsymbol{P}_{(2)}^{n-1} - \cdots - \boldsymbol{\mathcal{P}_K}\boldsymbol{P}_{(1)}^{n-K} - \boldsymbol{\mathcal{Q}_K}\boldsymbol{P}_{(2)}^{n-K} \tag{37}$$

where $\boldsymbol{u}^k$ and $\boldsymbol{v}^k$ denote the vector that contains all unknowns $\left\{u_j^k,\ j = 1, ..., N_e\right\}$ and $\left\{v_j^k,\ j = 1, ..., N_e\right\}$, respectively, at time level t_k. For N_e total surface elements, the non-zero entries of (34) are given by:

$$\begin{aligned}\boldsymbol{D_k} &= \left[\{\boldsymbol{D_k}\}_{ij}\right]_{N_e\times N_e} \text{ and } \{\boldsymbol{D_k}\}_{ij} = \delta_{ij}\rho_0\psi_{n-k}'(t_n)\\ \boldsymbol{E_k} &= \left[\{\boldsymbol{E_k}\}_{ij}\right]_{N_e\times N_e} \text{ and } \{\boldsymbol{E_k}\}_{ij} = \delta_{ij}\left(h_0\psi_{n-k}'(t_n) + R_0\psi_{n-k}(t_n)\right)\\ \boldsymbol{F_k} &= \left[\left\{\boldsymbol{F_k^{A_1}}\right\}_{ij} \cdots \left\{\boldsymbol{F_k^{A_{J_1}}}\right\}_{ij}\right]_{N_e\times J_1N_e} \text{ and } \left\{\boldsymbol{F_k^{A_\ell}}\right\}_{ij} = \delta_{ij}A_\ell\psi_{n-k}(t_n)\\ \boldsymbol{G_k} &= \left[\left\{\boldsymbol{G_k^{B_1}}\right\}_{ij} \cdots \left\{\boldsymbol{G_k^{B_{J_2}}}\right\}_{ij}\right]_{N_e\times J_2N_e} \text{ and } \left\{\boldsymbol{G_k^{B_\ell}}\right\}_{ij} = \delta_{ij}B_\ell\psi_{n-k}(t_n)\\ \boldsymbol{H_k} &= \left[\left\{\boldsymbol{H_k^{C_1}}\right\}_{ij} \cdots \left\{\boldsymbol{H_k^{C_{J_2}}}\right\}_{ij}\right]_{N_e\times J_2N_e} \text{ and } \left\{\boldsymbol{H_k^{C_\ell}}\right\}_{ij} = \delta_{ij}C_\ell\psi_{n-k}(t_n)\end{aligned}$$

where all matrices are diagonal.

Similarly, the non-zero entries of (35), (36), and (37) are given by:

$$\boldsymbol{\mathcal{J}_k} = \begin{bmatrix} \{\boldsymbol{\mathcal{J}_k}\}_{ij} \\ \mathbf{0} \\ \vdots \\ \mathbf{0} \end{bmatrix}_{J_1 N_e \times N_e} \quad \text{and} \quad \{\boldsymbol{\mathcal{J}_k}\}_{ij} = \delta_{ij}\psi_{n-k}(t_n)$$

$$\boldsymbol{\mathcal{K}_k} = \begin{bmatrix} \left\{\boldsymbol{\mathcal{K}_k^{\gamma_1}}\right\}_{ij} & & \\ & \ddots & \\ & & \left\{\boldsymbol{\mathcal{K}_k^{\gamma_{J_1}}}\right\}_{ij} \end{bmatrix}_{J_1 N_e \times J_1 N_e} \quad \text{and} \quad \left\{\boldsymbol{\mathcal{K}_k^{\gamma_\ell}}\right\}_{ij} = -\delta_{ij}\left(\psi'_{n-k}(t_n) + \gamma_\ell \psi_{n-k}(t_n)\right)$$

$$\boldsymbol{\mathcal{L}_k} = \begin{bmatrix} \{\boldsymbol{\mathcal{L}_k}\}_{ij} \\ \mathbf{0} \\ \vdots \\ \mathbf{0} \end{bmatrix}_{J_2 N_e \times N_e} \quad \text{and} \quad \{\boldsymbol{\mathcal{L}_k}\}_{ij} = \delta_{ij}\psi_{n-k}(t_n)$$

$$\boldsymbol{\mathcal{M}_k} = \begin{bmatrix} \left\{\boldsymbol{\mathcal{M}_k^{\alpha_1}}\right\}_{ij} & & \\ & \ddots & \\ & & \left\{\boldsymbol{\mathcal{M}_k^{\alpha_{J_2}}}\right\}_{ij} \end{bmatrix}_{J_2 N_e \times J_2 N_e} \quad \text{and} \quad \left\{\boldsymbol{\mathcal{M}_k^{\alpha_\ell}}\right\}_{ij} = -\delta_{ij}\left(\psi'_{n-k}(t_n) + \alpha_\ell \psi_{n-k}(t_n)\right)$$

$$\boldsymbol{\mathcal{N}_k} = \begin{bmatrix} \left\{\boldsymbol{\mathcal{N}_k^{\beta_1}}\right\}_{ij} & & \\ & \ddots & \\ & & \left\{\boldsymbol{\mathcal{N}_k^{\beta_{J_2}}}\right\}_{ij} \end{bmatrix}_{J_2 N_e \times J_2 N_e} \quad \text{and} \quad \left\{\boldsymbol{\mathcal{N}_k^{\beta_\ell}}\right\}_{ij} = -\delta_{ij}\beta_\ell \psi_{n-k}(t_n)$$

$$\boldsymbol{\mathcal{P}_k} = \begin{bmatrix} \left\{\boldsymbol{\mathcal{P}_k^{\beta_1}}\right\}_{ij} & & \\ & \ddots & \\ & & \left\{\boldsymbol{\mathcal{P}_k^{\beta_{J_2}}}\right\}_{ij} \end{bmatrix}_{J_2 N_e \times J_2 N_e} \quad \text{and} \quad \left\{\boldsymbol{\mathcal{P}_k^{\beta_\ell}}\right\}_{ij} = \delta_{ij}\beta_\ell \psi_{n-k}(t_n)$$

$$\boldsymbol{\mathcal{Q}_k} = \begin{bmatrix} \left\{\boldsymbol{\mathcal{Q}_k^{\alpha_1}}\right\}_{ij} & & \\ & \ddots & \\ & & \left\{\boldsymbol{\mathcal{Q}_k^{\alpha_{J_2}}}\right\}_{ij} \end{bmatrix}_{J_2 N_e \times J_2 N_e} \quad \text{and} \quad \left\{\boldsymbol{\mathcal{Q}_k^{\alpha_\ell}}\right\}_{ij} = -\delta_{ij}\left(\psi'_{n-k}(t_n) + \alpha_\ell \psi_{n-k}(t_n)\right)$$

where all matrices are diagonal. Further, in $\boldsymbol{\mathcal{J}_k}$, there are $(J_1 - 1)$ zero matrices $\mathbf{0}$ each with size $N_e \times N_e$ and, in $\boldsymbol{\mathcal{L}_k}$, there are $(J_2 - 1)$ zero matrices $\mathbf{0}$ each with size $N_e \times N_e$.

Coupling (34) through (32) with (13) forms a MOT scheme for the Burton-Miller-type TD-BIE using a broadband IBC. This coupled system has dimension $N_e(2 + J_1 + 2J_2) \times N_e(2 + J_1 + 2J_2)$ and is expressed as shown in (38). When solved iteratively, (38) provides solutions for $\boldsymbol{u}^k$ and $\boldsymbol{v}^k$ on rigid and soft surfaces.

$$
\begin{bmatrix} \boldsymbol{B_0} & \boldsymbol{C_0} & \boldsymbol{0} & \boldsymbol{0} & \boldsymbol{0} \\ \boldsymbol{D_0} & \boldsymbol{E_0} & \boldsymbol{F_0} & \boldsymbol{G_0} & \boldsymbol{H_0} \\ \boldsymbol{0} & \boldsymbol{\mathcal{J}_0} & \boldsymbol{\mathcal{K}_0} & \boldsymbol{0} & \boldsymbol{0} \\ \boldsymbol{0} & \boldsymbol{\mathcal{L}_0} & \boldsymbol{0} & \boldsymbol{\mathcal{M}_0} & \boldsymbol{\mathcal{N}_0} \\ \boldsymbol{0} & \boldsymbol{0} & \boldsymbol{0} & \boldsymbol{\mathcal{P}_0} & \boldsymbol{\mathcal{Q}_0} \end{bmatrix} \begin{bmatrix} \boldsymbol{u^n} \\ \boldsymbol{v^n} \\ \boldsymbol{P^n_{(0)}} \\ \boldsymbol{P^n_{(1)}} \\ \boldsymbol{P^n_{(2)}} \end{bmatrix}
$$

$$
= \begin{bmatrix} \boldsymbol{q^n} \\ \boldsymbol{0} \\ \boldsymbol{0} \\ \boldsymbol{0} \\ \boldsymbol{0} \end{bmatrix} - \begin{bmatrix} \boldsymbol{B_1} & \boldsymbol{C_1} & \boldsymbol{0} & \boldsymbol{0} & \boldsymbol{0} \\ \boldsymbol{D_1} & \boldsymbol{E_1} & \boldsymbol{F_1} & \boldsymbol{G_1} & \boldsymbol{H_1} \\ \boldsymbol{0} & \boldsymbol{\mathcal{J}_1} & \boldsymbol{\mathcal{K}_1} & \boldsymbol{0} & \boldsymbol{0} \\ \boldsymbol{0} & \boldsymbol{\mathcal{L}_1} & \boldsymbol{0} & \boldsymbol{\mathcal{M}_1} & \boldsymbol{\mathcal{N}_1} \\ \boldsymbol{0} & \boldsymbol{0} & \boldsymbol{0} & \boldsymbol{\mathcal{P}_1} & \boldsymbol{\mathcal{Q}_1} \end{bmatrix} \begin{bmatrix} \boldsymbol{u^{n-1}} \\ \boldsymbol{v^{n-1}} \\ \boldsymbol{P^{n-1}_{(0)}} \\ \boldsymbol{P^{n-1}_{(1)}} \\ \boldsymbol{P^{n-1}_{(2)}} \end{bmatrix} - \begin{bmatrix} \boldsymbol{B_2} & \boldsymbol{C_2} & \boldsymbol{0} & \boldsymbol{0} & \boldsymbol{0} \\ \boldsymbol{D_2} & \boldsymbol{E_2} & \boldsymbol{F_2} & \boldsymbol{G_2} & \boldsymbol{H_2} \\ \boldsymbol{0} & \boldsymbol{\mathcal{J}_2} & \boldsymbol{\mathcal{K}_2} & \boldsymbol{0} & \boldsymbol{0} \\ \boldsymbol{0} & \boldsymbol{\mathcal{L}_2} & \boldsymbol{0} & \boldsymbol{\mathcal{M}_2} & \boldsymbol{\mathcal{N}_2} \\ \boldsymbol{0} & \boldsymbol{0} & \boldsymbol{0} & \boldsymbol{\mathcal{P}_2} & \boldsymbol{\mathcal{Q}_2} \end{bmatrix} \begin{bmatrix} \boldsymbol{u^{n-2}} \\ \boldsymbol{v^{n-2}} \\ \boldsymbol{P^{n-2}_{(0)}} \\ \boldsymbol{P^{n-2}_{(1)}} \\ \boldsymbol{P^{n-2}_{(2)}} \end{bmatrix} \tag{38}
$$

$$
- \cdots - \begin{bmatrix} \boldsymbol{B_K} & \boldsymbol{C_K} & \boldsymbol{0} & \boldsymbol{0} & \boldsymbol{0} \\ \boldsymbol{D_K} & \boldsymbol{E_K} & \boldsymbol{F_K} & \boldsymbol{G_K} & \boldsymbol{H_K} \\ \boldsymbol{0} & \boldsymbol{\mathcal{J}_K} & \boldsymbol{\mathcal{K}_K} & \boldsymbol{0} & \boldsymbol{0} \\ \boldsymbol{0} & \boldsymbol{\mathcal{L}_K} & \boldsymbol{0} & \boldsymbol{\mathcal{M}_K} & \boldsymbol{\mathcal{N}_K} \\ \boldsymbol{0} & \boldsymbol{0} & \boldsymbol{0} & \boldsymbol{\mathcal{P}_K} & \boldsymbol{\mathcal{Q}_K} \end{bmatrix} \begin{bmatrix} \boldsymbol{u^{n-K}} \\ \boldsymbol{v^{n-K}} \\ \boldsymbol{P^{n-K}_{(0)}} \\ \boldsymbol{P^{n-K}_{(1)}} \\ \boldsymbol{P^{n-K}_{(2)}} \end{bmatrix} - \cdots - \begin{bmatrix} \boldsymbol{B_J} & \boldsymbol{C_J} & \boldsymbol{0} & \boldsymbol{0} & \boldsymbol{0} \\ \boldsymbol{0} & \boldsymbol{0} & \boldsymbol{0} & \boldsymbol{0} & \boldsymbol{0} \\ \boldsymbol{0} & \boldsymbol{0} & \boldsymbol{0} & \boldsymbol{0} & \boldsymbol{0} \\ \boldsymbol{0} & \boldsymbol{0} & \boldsymbol{0} & \boldsymbol{0} & \boldsymbol{0} \end{bmatrix} \begin{bmatrix} \boldsymbol{u^{n-J}} \\ \boldsymbol{v^{n-J}} \\ \boldsymbol{P^{n-J}_{(0)}} \\ \boldsymbol{P^{n-J}_{(1)}} \\ \boldsymbol{P^{n-J}_{(2)}} \end{bmatrix}
$$

IV. Numerical Eigenvalue Study and Stability Analysis

The solution of the MOT scheme (38) provides a prediction of the acoustic scattering around a body from a given noise source. To assess the stability this system, a numerical eigenvalue study is conducted. Denote (38) by:

$$
\boldsymbol{A_0 w^n} = \boldsymbol{q_0^n} - \boldsymbol{A_1 w^{n-1}} - \boldsymbol{A_2 w^{n-2}} - \ldots - \boldsymbol{A_K w^{n-K}} - \ldots - \boldsymbol{A_J w^{n-J}} \tag{39}
$$

where

$$
\boldsymbol{A_k} = \begin{bmatrix} \boldsymbol{B_K} & \boldsymbol{C_K} & \boldsymbol{0} & \boldsymbol{0} & \boldsymbol{0} \\ \boldsymbol{D_K} & \boldsymbol{E_K} & \boldsymbol{F_K} & \boldsymbol{G_K} & \boldsymbol{H_K} \\ \boldsymbol{0} & \boldsymbol{\mathcal{J}_K} & \boldsymbol{\mathcal{K}_K} & \boldsymbol{0} & \boldsymbol{0} \\ \boldsymbol{0} & \boldsymbol{\mathcal{L}_K} & \boldsymbol{0} & \boldsymbol{\mathcal{M}_K} & \boldsymbol{\mathcal{N}_K} \\ \boldsymbol{0} & \boldsymbol{0} & \boldsymbol{0} & \boldsymbol{\mathcal{P}_K} & \boldsymbol{\mathcal{Q}_K} \end{bmatrix}_{k=0,\ldots,K}, \quad \boldsymbol{A_k} = \begin{bmatrix} \boldsymbol{B_K} & \boldsymbol{0} & \boldsymbol{0} & \boldsymbol{0} & \boldsymbol{0} \\ \boldsymbol{0} & \boldsymbol{0} & \boldsymbol{0} & \boldsymbol{0} & \boldsymbol{0} \\ \boldsymbol{0} & \boldsymbol{0} & \boldsymbol{0} & \boldsymbol{0} & \boldsymbol{0} \\ \boldsymbol{0} & \boldsymbol{0} & \boldsymbol{0} & \boldsymbol{0} & \boldsymbol{0} \\ \boldsymbol{0} & \boldsymbol{0} & \boldsymbol{0} & \boldsymbol{0} & \boldsymbol{0} \end{bmatrix}_{k=K+1,\ldots,J}, \quad \boldsymbol{w^n} = \begin{bmatrix} \boldsymbol{u^n} \\ \boldsymbol{v^n} \\ \boldsymbol{P^n_{(0)}} \\ \boldsymbol{P^n_{(1)}} \\ \boldsymbol{P^n_{(2)}} \end{bmatrix}, \quad \boldsymbol{q_0^n} = \begin{bmatrix} \boldsymbol{q^n} \\ \boldsymbol{0} \\ \boldsymbol{0} \\ \boldsymbol{0} \\ \boldsymbol{0} \end{bmatrix}.
$$

For the stability study, the eigenvalue analyses is concerned only with the homogeneous system. The homogeneous system is representative of when the source, or incident wave, has traveled far beyond the scattering body and it is often when numerical instability occurs. Seeking solutions of the form $\boldsymbol{w^n} = \lambda^n \boldsymbol{e_0}$ to the corresponding homogeneous system (39), a polynomial eigenvalue problem is obtained:

$$
\left[\boldsymbol{A_0} \lambda^J + \boldsymbol{A_1} \lambda^{J-1} + \boldsymbol{A_2} \lambda^{J-2} + \cdots + \boldsymbol{A_{J-1}} \lambda + \boldsymbol{A_J} \right] \boldsymbol{e_0} = 0. \tag{40}
$$

Equation (40) is cast into a generalized eigenvalue problem with eigenvectors $\boldsymbol{e}_j = \lambda^j \boldsymbol{e}_0 = \lambda \boldsymbol{e}_{j-1}$. The largest eigenvalue $\lambda_{\max}$ of the generalized eigenvalue problem is then calculated by using a matrix power iteration method as detailed in Appendix A. The matrix power method is run using code written in Matlab and is repeated until the iterative scheme has converged to the largest eigenvalue, $|\lambda|_{\max}$, *i.e.*, when $|\lambda^{(k)} - \lambda^{(k-1)}|/|\lambda^{(k)}| < \delta$ for a given tolerance δ as detailed in Appendix A. If the numerical scheme given by (39) is stable, it is necessary that $|\lambda_{\max}| \leq 1$ for all λ in (40) [2, 29, 49–51].

The stability of the numerical algorithm is investigated by considering the scattering of an acoustic point source by a flat plate with dimension $[-0.5, 0.5] \times [-0.5, 0.5] \times [-0.1, 0.1]$. The acoustic point source, located at $\boldsymbol{x} = (0, 0, 1)$, is centered directly above the body as illustrated in Figure 2. The surface of the flat plate is discretized in the x-, y-, and z-directions with N_x, N_y, and N_z elements, respectively, giving a total number of $N_e = 2(N_x N_y + N_y N_z + N_x N_z)$ surface elements. Three problem sizes of $N_x \times N_y \times N_z$ are considered: $5 \times 5 \times 1$ ($N_e = 70$ elements), $10 \times 10 \times 2$ ($N_e = 280$ elements), and $20 \times 20 \times 4$ ($N_e = 1,120$ elements) as illustrated in Figures 3a through 3c.

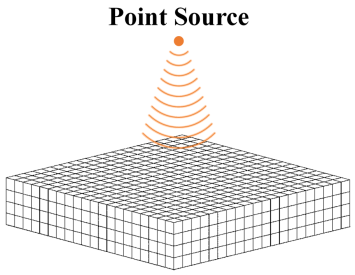

Fig. 2 Illustration of the radiative scattering by a flat plate.

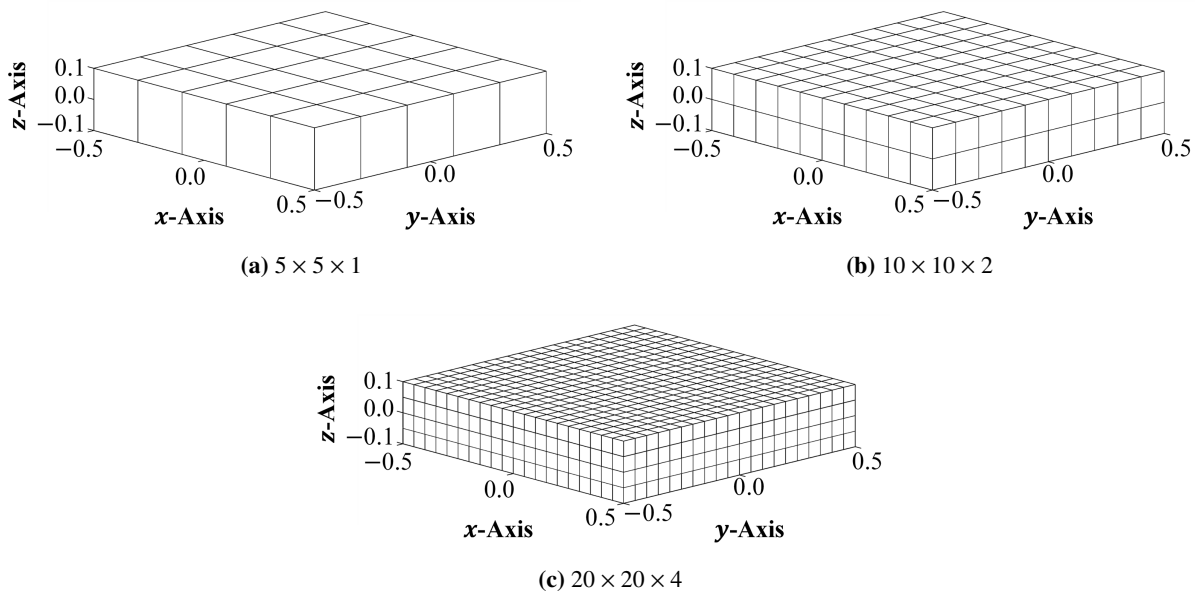

(a) $5 \times 5 \times 1$ **(b)** $10 \times 10 \times 2$

(c) $20 \times 20 \times 4$

Fig. 3 Schematic diagrams illustrating the respective discretization for the flat plate with dimension $[-0.5, 0.5] \times [-0.5, 0.5] \times [-0.1, 0.1]$ **used for modeling the acoustic scattering of a point source located at** $(x, y, z) = (0, 0, 1)$**.**

In [51], the authors considered time steps of $\Delta t = \pi/1000$ and $\Delta t = 1/24$ for discretizations $10 \times 10 \times 2$ through $30 \times 30 \times 6$ when studying the *Extended Helmholtz Resonator Model* with third-order temporal basis functions (12). Further, when using Burton-Miller-type reformulation with (12), stability has been demonstrated using as little as 22 points per wave period [36], translating to a minimum time step of $\Delta t \approx \Delta x$. Wanting to ensure large enough time steps for the given basis functions (12), the authors then considered time steps of $\Delta t = 1/12$ and $\Delta t = 1/24$ for discretizations $10 \times 10 \times 2$ through $30 \times 30 \times 6$ when studying both the *Extended Helmholtz Resonator Model* and the *Broadband Impedance Model* in [2]. It was found that the stability tends to improve as the spatial grid is refined indicating that a spatial resolution of $N_x = 30$ is sufficiently fine for the third-order temporal basis functions, and that for the coarser grids, $N_x = 10$ and $N_x = 20$, a larger time step may be required to ensure $\Delta t \approx \Delta x$, at a minimum. Following from these previous analyses, the authors now consider coarser grids ($N_x = 5, 10, 20$ rather than $N_x = 10, 20, 30$) with time steps of $\Delta t = 1/12$ and $\Delta t = 1/24$ for modeling the *Broadband Impedance Model* liner boundary condition with both a second-order and third-order implicit backward difference temporal scheme, BD2 and BD3. Considering both time steps ensures that the scattering problem provides solutions over a wide range of frequencies as is desired for broadband noise prediction, allows for the ability to assess the dependence of time step on stability, and further allows for the consideration of a coarser grid than was studied in both [51] and [2]: $5 \times 5 \times 1$.

For the *Broadband Impedance Model*, the liner boundary condition is modeled using experimental data. Two acoustic liners, named CT57 and GE03, were tested in the Grazing Flow Impedance Tube at the NASA Langley Research Center Liner Technology Facility [58]. During the tests [59], impedance values were measured along a wide range of

frequencies. Using the measured data, five different numerical models were generated using least squares regression giving values for the parameters which define the surface impedance (17): $h_0, R_0, J_1, A_\ell, \gamma_\ell, J_2, B_\ell, C_\ell, \alpha_\ell, \beta_\ell$. In each of the numerical models, herein referred to as Cases 1 through 5, the parameters yield $\mathrm{Re}(Z) > 0$, thus preserving causality and stability. This representation is not unique and merely represents five different possible options. Table 1 lists all of the constants generated for this model, and Figures 4a and 4b illustrate two such examples: Cases 1 and 4. Figure 4a depicts experimental data from the CT57 liner and Figure 4b depicts experimental data from the GE03. In each figure, the experimental data is graphed using solid circles and the numerical model is graphed with a dotted line. The CT57 liner is modeled using Cases 1, 2, and 3. The GE03 liner is modeled using Cases 4 and 5.

Table 1 Constants used for the *Broadband Impedance Model*.

Case	h_0	R_0	J_1	A_ℓ	γ_ℓ	J_2	B_ℓ	C_ℓ	α_ℓ	β_ℓ
				$\ell = 1, \ldots, J_1$			$\ell = 1, \ldots, J_2$			
1 (CT57)	0.010873	0.177655	1	18.467174	0.985273	2	43.919202	-0.571804	4.887694	37.631479
							23.611034	-8.511097	7.670216	-66.460858
2 (CT57)	0	0	1	18.422293	1.091586	2	98.624933	-3.063868	6.641055	81.958998
							44.048396	-0.696846	4.871120	37.450376
3 (CT57)	0	0.068743	1	18.421975	1.075243	2	99.855347	-9.968384	7.952528	82.203159
							44.089363	-0.709128	4.879110	37.451098
4 (GE03)	0.011775	0.001514	1	32.573728	1.896347	2	0.001101	-9.910991	22.599229	16.476064
							75.213211	-9.915633	7.374808	82.791519
5 (GE03)	0	0	1	27.493859	0.470593	3	99.686994	1.823551	10.638159	96.074097
							99.672009	-9.863166	0.080378	97.146410
							1.066955	0.959000	1.137323	7.645146

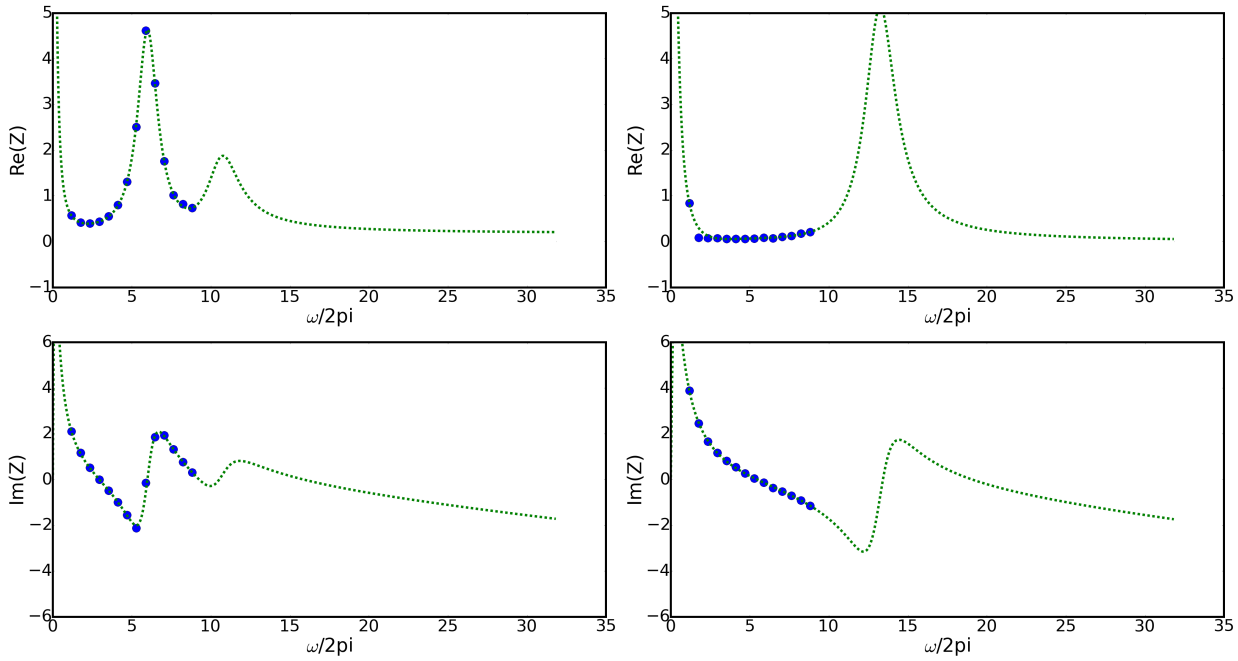

(a) Broadband Case 1 **(b) Broadband Case 4**

Fig. 4 Illustration of the generated *Broadband Impedance Model* impedance curves using least squares regression. The experimental data is graphed using solid circles and the numerical model is graphed with a dotted line. The left graph is of the CT57 liner and the right graph is of the GE03 liner.

For the stability assessment, two different applications of an acoustic liner are considered. First, it is assumed that the acoustic liner is installed on all scattering surfaces. Herein referred to as "*soft*," this configuration is illustrated in Figure 5a. It is further assumed that is acoustic liner is installed on the top-surface of the flat plate nearest the point source (refer to Figure 2). Herein referred to as "*mixed*," this configuration is illustrated in Figure 5b. For reference, the flat plates illustrated in Figure 3 are for rigid body scattering, *i.e.*, no acoustic liner. Using the rigid body as a baseline, the stability of the numerical algorithm is tested assuming no liner boundary condition on any scattering surface. Then, both *soft* and *mixed* body liner applications are assessed for their stability in solving the system (39). With no liner installed on the scattering surface, all baseline cases are expected to yield eigenvalues no greater than unity. For the baseline assessment, all matrices associated with the liner boundary condition are equivalently set equal to zero.

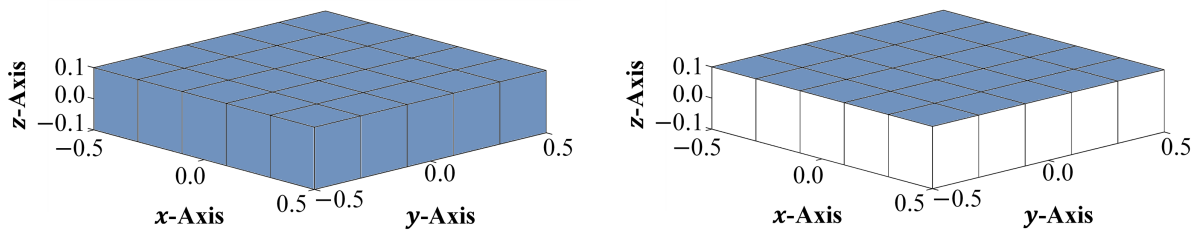

(a) Soft Body **(b) Mixed Body**

Fig. 5 Schematic diagrams illustrating a comparison between a fully-lined and a partially-lined scattering body for a flat plate with discretization $5 \times 5 \times 1$**.**

The values of the maximum eigenvalue for the *rigid*, *soft*, and *mixed* bodies are calculated using a code written in Matlab. All *soft* eigenvalue results are listed in Table 2. All *mixed* eigenvalue results are listed in Table 3. The *rigid* body results are not listed in table form because, as expected, all baseline cases yield a maximum eigenvalue of 1.000000 for all discretizations $5\times5\times1$, $10\times10\times2$, and $20\times20\times4$, time steps $\Delta t = 1/12$ and $\Delta t = 1/24$, and temporal basis functions BD2 and BD3. Since $|\lambda_{\max}| \leq 1$ for all λ, the baseline study validates that the Burton-Miller-type reformulation of the TD-BIE provides numerical stability by successfully eliminating resonant frequencies.

All eigenvalues in Tables 2 and 3 converge to a tolerance $\delta < 10^{-9}$ within 5,000 iterations (refer to Appendix A). Any eigenvalues greater than unity are listed in **bold**. For *soft* body scattering, Table 2, the analysis demonstrates stability in three out of five numerical models. Apart from Cases 4 and 5, all analyses yield a maximum eigenvalue no greater than unity. For *mixed* body scattering, Table 3, the analysis demonstrates stability in four out of five numerical models. Apart from Case 4, all analyses yield a maximum eigenvalue no greater than unity. Moreover, it is also worth mentioning that in all of the unstable cases, the maximum eigenvalue is only slightly larger than unity.

In both the *soft* and *mixed* body analyses, Case 4 is largely unstable providing maximum eigenvalues greater than unity for most assessments. The results indicate that stability can be realized when both the time step is small and the discretization is fine. Case 5 further demonstrates that stability can be realized as the discretization is refined for fully-lined bodies. These results are consistent with previous work [2, 51] where it was found that the stability tends to improve as the spatial grid is refined and that, for the coarser grids, a larger time step may be required to ensure $\Delta t \approx \Delta x$, at a minimum. Comparing the order of the temporal basis functions, there is little difference between BD2 and BD3 for fully-lined bodies. There is also little difference for partially-lined bodies with a larger time step, but for partially-lined bodies with a smaller time step, BD3 is more stable than BD2. However, though the choice of time step, discretization, and temporal order affect the stability, it is more likely that stability is dependent on the specific numerical parameters developed from the experimental data. Of the two numerical models developed for the GE03 liner, *e.g.*, Cases 4 and 5, one is largely stable whereas the other is not.

From the results shown Tables 2 and 3, it can be concluded that the *Broadband* model is sufficient for predicting scattering by bodies with lined surfaces. This assessment demonstrates that eigenvalue analysis, though not a sufficient condition for stability, is necessary. Thus, if additional acoustic liners are tested experimentally and numerical models developed, it is pertinent that each case is assessed for its stability prior to predicting the acoustic wave scattering using the *Broadband Impedance Model* while noting that for stability, it is required that resistance is a positive value.

Table 2 Maximum eigenvalues calculated for the *Broadband Impedance Model* assuming the liner installed on all scattering surfaces (*soft* body scattering).

Basis Function	*Broadband Model*	$\Delta t = 1/12$			$\Delta t = 1/24$		
		$5 \times 5 \times 1$	$10 \times 10 \times 2$	$20 \times 20 \times 4$	$5 \times 5 \times 1$	$10 \times 10 \times 2$	$20 \times 20 \times 4$
BD2	Case 1	1.000000	1.000000	1.000000	1.000000	1.000000	1.000000
	Case 2	1.000000	1.000000	1.000000	1.000000	1.000000	1.000000
	Case 3	1.000000	1.000000	1.000000	1.000000	1.000000	1.000000
	Case 4	0.999990	**1.000276**	**1.000165**	**1.000069**	**1.000024**	0.999990
	Case 5	1.000000	1.000000	1.000000	**1.000004**	1.000000	1.000000
BD3	Case 1	1.000000	1.000000	1.000000	1.000000	1.000000	1.000000
	Case 2	1.000000	1.000000	1.000000	1.000000	1.000000	1.000000
	Case 3	1.000000	1.000000	1.000000	1.000000	1.000000	1.000000
	Case 4	0.999976	**1.000231**	**1.000116**	**1.000017**	0.999965	0.999967
	Case 5	**1.000006**	1.000000	1.000000	**1.000026**	1.000000	1.000000

Table 3 Maximum eigenvalues calculated for the *Broadband Impedance Model* assuming the liner installed on the top-most scattering surfaces (*mixed* body scattering).

Basis Function	*Broadband Model*	$\Delta t = 1/12$			$\Delta t = 1/24$		
		$5 \times 5 \times 1$	$10 \times 10 \times 2$	$20 \times 20 \times 4$	$5 \times 5 \times 1$	$10 \times 10 \times 2$	$20 \times 20 \times 4$
BD2	Case 1	1.000000	1.000000	1.000000	1.000000	1.000000	1.000000
	Case 2	1.000000	1.000000	1.000000	1.000000	1.000000	1.000000
	Case 3	1.000000	1.000000	1.000000	1.000000	1.000000	1.000000
	Case 4	**1.000505**	**1.000218**	**1.000101**	**1.000123**	**1.000052**	**1.000003**
	Case 5	1.000000	1.000000	1.000000	1.000000	1.000000	0.996639
BD3	Case 1	1.000000	1.000000	1.000000	1.000000	1.000000	1.000000
	Case 2	1.000000	1.000000	1.000000	1.000000	1.000000	1.000000
	Case 3	1.000000	1.000000	1.000000	1.000000	1.000000	1.000000
	Case 4	**1.000148**	**1.000173**	**1.000073**	0.999999	0.999981	0.999991
	Case 5	1.000000	0.993455	1.000000	1.000000	1.000000	0.996639

V. Concluding Remarks

Reducing aircraft noise is a major objective in the field of computational aeroacoustics. When designing next generation quiet aircraft, it is important to be able to accurately and efficiently predict the acoustic scattering by an aircraft body from a given noise source. Acoustic scattering problems can be modeled using BEMs by reformulating the linear convective wave equation as a TD-BIE, both in the frequency-domain and the time-domain. Time-domain solvers allow for the simulation and study of broadband sources and time-dependent transient signals, for the scattering solutions at all frequencies to be obtained within a single computation, and for the ability to more naturally coupled with a nonlinear computational fluid dynamics simulation of noise sources.

TD-BIEs unfortunately have an intrinsic numerical instability. This instability is observed across multiple disciplines and is a result of internal modes of resonance corresponding to time harmonic solutions of the integral equation [32]. These resonant modes yield an ill-conditioned matrix in the frequency-domain due to the existence of non-unique solutions which results in numerical instability in the time-domain [4, 33]. In recent years, numerical techniques for modeling acoustic wave scattering using TD-BIEs have been under development [1, 36–38]. It has been shown that stability can be realized through implementing a Burton-Miller-type reformulation of the TD-BIE and both computational cost and computational time can be reduced using fast algorithms and high performance computing.

The objective of this study was to investigate the feasibility and stability for modeling acoustic wave scattering using a Burton-Miller-type TD-BIE with IBC. In Section II, the derivation of a TD-BIE, stabilized through a Burton-Miller-type reformulation, was presented and in Section III, the IBC was derived and the *Broadband Impedance Model* was introduced. This model is a numerical representation of the impedance provided by an acoustic liner. Typically composed of an array of Helmholtz resonators, acoustic liners are installed on the surfaces of scattering bodies and are incredibly effective at suppressing noise.

In Section IV, the stability of the Burton-Miller-type TD-BIE coupled with a liner boundary condition was assessed. In literature, stability analysis has proven convolution quadrature methods second-order convergent for basis functions constant in space and linear in time [48], but no theoretical proof has yet been provided for other methods. Eigenvalue analysis is the current standard for studying the stability of TD-BIEs [29, 49, 50]. In this work, eigenvalue analysis was conducted for the *Broadband* model assuming both fully- and partially-lined bodies. Though not a sufficient condition for proving stability, it is necessary that the magnitude of all eigenvalues is no greater than unity for stability to be achieved.

The *Broadband Impedance Model* eigenvalue analyses demonstrated stability for both the fully- and partially-lined bodies in most cases. In both the *soft* and *mixed* body analyses, Case 4 is largely unstable. The results indicate that stability can be realized when both the time step is small and the discretization is fine. Case 5 further demonstrated that stability can be realized as the discretization is refined for fully-lined bodies. These results are consistent with previous work [2, 51] where two different single frequency impedance models were considered for representing the acoustic liner: the *Extended Helmholtz Resonator Model* and the *Three-Parameter Impedance Model*. The *Broadband* results also indicated little dependence on the order of the temporal basis function except for partially-lined bodies with a smaller time step where it was demonstrated that BD3 was more stable than BD2.

The *Broadband* results further indicate that it is more likely that stability is dependent on the specific numerical parameters developed from the experimental data. These results reinforce that eigenvalue analysis is necessary to fully assess the stability of a numerical scheme. Understanding the stability of such a model improves the capabilities of designing next generation quieter aircraft.

Acknowledgments

F. Q. Hu and M. E. Rodio are supported by a NASA Cooperative Agreement, NNX11AI63A. M. E. Rodio is also supported in part by a Virginia Space Grant Consortium Graduate Fellowship as part of her doctoral program. This work used the computational resources at the Old Dominion University ITS Turing Cluster and the Extreme Science and Engineering Discovery Environment, which is supported by National Science Foundation grant number OCI-1053575.

Appendix A: Matrix Power Iteration Method

In this appendix, the methodology for solving a polynomial eigenvalue problem using a matrix power iteration method is discussed. Seeking solutions of the form $\boldsymbol{w^n} = \lambda^n \boldsymbol{e}_0$ to the corresponding homogeneous system (39) yields the polynomial eigenvalue problem given by (40) in Section IV:

$$\left[\boldsymbol{A_0}\lambda^J + \boldsymbol{A_1}\lambda^{J-1} + \boldsymbol{A_2}\lambda^{J-2} + \cdots + \boldsymbol{A_{J-1}}\lambda + \boldsymbol{A_J}\right]\boldsymbol{e}_0 = 0$$

where $\boldsymbol{e}_j = \lambda^j \boldsymbol{e}_0 = \lambda \boldsymbol{e}_{j-1}$ for all $j = 1, \ldots, J$, *i.e.*,

$$\boldsymbol{A_0}\lambda\boldsymbol{e}_{J-1} + \boldsymbol{A_1}\boldsymbol{e}_{J-1} + \boldsymbol{A_2}\boldsymbol{e}_{J-2} + \cdots + \boldsymbol{A_{J-1}}\boldsymbol{e}_1 + \boldsymbol{A_J}\boldsymbol{e}_0 = 0. \tag{41}$$

Equation (41) is then cast into a generalized eigenvalue problem:

$$\lambda \begin{bmatrix} \boldsymbol{A_0} & 0 & 0 & \cdots & 0 & 0 \\ 0 & \boldsymbol{I} & 0 & \cdots & 0 & 0 \\ 0 & 0 & \boldsymbol{I} & \cdots & 0 & 0 \\ \vdots & \vdots & & \ddots & & \vdots \\ 0 & 0 & 0 & \cdots & \boldsymbol{I} & 0 \\ 0 & 0 & 0 & \cdots & 0 & \boldsymbol{I} \end{bmatrix} \begin{bmatrix} \boldsymbol{e_{J-1}} \\ \boldsymbol{e_{J-2}} \\ \boldsymbol{e_{J-3}} \\ \vdots \\ \boldsymbol{e_1} \\ \boldsymbol{e_0} \end{bmatrix} = \begin{bmatrix} -\boldsymbol{A_1} & -\boldsymbol{A_2} & \cdots & -\boldsymbol{A_{J-2}} & -\boldsymbol{A_{J-1}} & -\boldsymbol{A_J} \\ \boldsymbol{I} & 0 & \cdots & 0 & 0 & 0 \\ 0 & \boldsymbol{I} & \cdots & 0 & 0 & 0 \\ \vdots & & \ddots & & \vdots & \vdots \\ 0 & 0 & \cdots & \boldsymbol{I} & 0 & 0 \\ 0 & 0 & \cdots & 0 & \boldsymbol{I} & 0 \end{bmatrix} \begin{bmatrix} \boldsymbol{e_{J-1}} \\ \boldsymbol{e_{J-2}} \\ \vdots \\ \boldsymbol{e_2} \\ \boldsymbol{e_1} \\ \boldsymbol{e_0} \end{bmatrix}.$$

Simplifying gives:

$$\lambda \begin{bmatrix} \boldsymbol{e_{J-1}} \\ \boldsymbol{e_{J-2}} \\ \boldsymbol{e_{J-3}} \\ \vdots \\ \boldsymbol{e_1} \\ \boldsymbol{e_0} \end{bmatrix} = \begin{bmatrix} -\boldsymbol{A_0}^{-1}\boldsymbol{A_1} & -\boldsymbol{A_0}^{-1}\boldsymbol{A_2} & \cdots & -\boldsymbol{A_0}^{-1}\boldsymbol{A_{J-2}} & -\boldsymbol{A_0}^{-1}\boldsymbol{A_{J-1}} & -\boldsymbol{A_0}^{-1}\boldsymbol{A_J} \\ \boldsymbol{I} & 0 & \cdots & 0 & 0 & 0 \\ 0 & \boldsymbol{I} & \cdots & 0 & 0 & 0 \\ \vdots & & \ddots & & \vdots & \vdots \\ 0 & 0 & \cdots & \boldsymbol{I} & 0 & 0 \\ 0 & 0 & \cdots & 0 & \boldsymbol{I} & 0 \end{bmatrix} \begin{bmatrix} \boldsymbol{e_{J-1}} \\ \boldsymbol{e_{J-2}} \\ \vdots \\ \boldsymbol{e_2} \\ \boldsymbol{e_1} \\ \boldsymbol{e_0} \end{bmatrix},$$

which can then be written as

$$\boldsymbol{A}\boldsymbol{e} = \lambda \boldsymbol{e}. \tag{42}$$

The matrix power iteration method is then used to find the largest eigenvalue of (42). The method proceeds as follows:
Step 1) Define an arbitrary unit vector to be $\boldsymbol{\xi}^{(0)}$.
Step 2) For $k = 1, 2, \ldots,$ calculate

$$\boldsymbol{e}^{(k)} = \boldsymbol{A}\boldsymbol{\xi}^{(k-1)}, \boldsymbol{q}^{(k)} = \frac{\boldsymbol{e}^{(k)}}{||\boldsymbol{e}^{(k)}||_2}, \text{ and } \lambda^{(k)} = \left[\boldsymbol{\xi}^{(k)}\right]^T \boldsymbol{A}\boldsymbol{\xi}^{(k)} = \left[\boldsymbol{\xi}^{(k)}\right]^T \boldsymbol{e}^{(k+1)}.$$

Step 3) Calculate the difference between consecutive eigenvalues, $|\lambda^{(k)} - \lambda^{(k-1)}|$.
Step 4) Repeat until the iterative scheme has converged to the largest eigenvalue, $|\lambda|_{\max}$, *i.e.*, when $|\lambda^{(k)} - \lambda^{(k-1)}|/|\lambda^{(k)}| < \delta$ for a given tolerance δ.

Herein, the following limitations are set for the tolerance δ in order to ensure that the matrix power iteration method returns a converged solution within a reasonable amount of iterations: if iterations $< 5,000$ then $\delta = 10^{-9}$ and if iterations $\geq 5,000$ then the solution is considered non-convergent.

References

[1] Hu, F. Q., "An Efficient Solution of Time-Domain Boundary Integral Equations for Acoustic Scattering and Its Acceleration by Graphics Processing Units," *19th AIAA/CEAS Aeroacoustics Conference*, American Institute of Aeronautics and Astronautics, AIAA paper 2013–2018, 2013.

[2] Rodio, M. E., Hu, F. Q., and Nark, D. M., "Investigating the Numerical Stability of a Time-Domain Boundary Integral Equation with Impedance Boundary Condition for Simulating Sound Absorption of Lined Bodies," *25th AIAA/CEAS Aeroacoustics Conference*, American Institute of Aeronautics and Astronautics, AIAA paper 2019–2416, 2019.

[3] Chappell, D. J., Harris, P. J., Henwood, D., and Chakrabarti, R., "A Stable Boundary Element Method for Modeling Transient Acoustic Radiation," *Journal of the Acoustical Society of America*, Vol. 120, No. 1, 2006, pp. 74–80.

[4] Ergin, A. A., Shankar, B., and Michielssen, E., "Analysis of Transient Wave Scattering from Rigid Bodies Using a Burton-Miller Approach," *Journal of the Acoustical Society of America*, Vol. 106, No. 5, 1999, pp. 2396–2404.

[5] Jones, A. D., and Hu, F. Q., "A Three-Dimensional Time-Domain Boundary Element Method for the Computation of Exact Green's Functions in Acoustic Analogy," *13th AIAA/CEAS Aeroacoustics Conference*, American Institute of Aeronautics and Astronautics, AIAA paper 2007–3479, 2007.

[6] Marburg, S., "The Burton and Miller Method: Unlocking Another Mystery of Its Coupling Parameter," *Journal of Computational Acoustics*, Vol. 23, No. 1550016, 2015.

[7] Marburg, S., and Schneider, S., "Influence of Element Types on Numeric Error for Acoustic Boundary Elements," *Journal of Computational Acoustics*, Vol. 11, No. 3, 2001, pp. 363–386.

[8] Astley, R. J., and Macaulay, G. J., "Three-Dimensional Wave-Envelope Elements of Variable Order for Acoustic Radiation and Scattering, Part I: Formulation in the Frequency-Domain," *Journal of the Acoustical Society of America*, Vol. 103, No. 1, 1998, pp. 49–63.

[9] Astley, R. J., and Bain, J. G., "A Three-Dimensional Boundary Element Scheme for Acoustic Radiation in Low Mach Number Flows," *Journal of Sound and Vibration*, Vol. 109, No. 3, 1986, pp. 445–465.

[10] Johnston, R. L., and Fairweather, G., "The Method of Fundamental Solutions for Problems in Potential Flow," *Applied Mathematical Modelling*, Vol. 8, No. 4, 1984, pp. 265–270.

[11] Wu, S. F., and Yu, J., "Reconstructing Interior Acoustic Pressure Fields via Helmholtz Equation Least-Squares Method," *Journal of the Acoustical Society of America*, Vol. 104, No. 4, 1998, pp. 2054–2060.

[12] Kamiya, N., Andoh, E., and Nogae, K., "Eigenvalue Analysis by the Boundary Element Method: New Developments," *Engineering Analysis with Boundary Elements*, Vol. 12, No. 3, 1993, pp. 151–162.

[13] Tsao, W. H., and Hwang, W. S., "Regularized Boundary Integral Methods for Three-Dimensional Potential Flows," *Engineering Analysis with Boundary Elements*, Vol. 77, No. 1, 2017, pp. 49–60.

[14] Shaw, R. P., "Transient Scattering by a Circular Cylinder," *Journal of Sound and Vibration*, Vol. 42, No. 3, 1975, pp. 295–304.

[15] Ffowcs-Williams, J. E., and Hawkings, D. L., "Sound Generation by Turbulence and Surfaces in Arbitrary Motion," *Philosophical Transactions of the Royal Society of London*, Vol. 264, No. 1151, 1969, pp. 321–342.

[16] Farassat, F., "Discontinuities in Aerodynamics and Aeroacoustics: The Concept and Applications of Generalized Derivatives," *Journal of Sound and Vibration*, Vol. 55, No. 2, 1977, pp. 165–193.

[17] Farassat, F., and Meyers, M. K., "Extension of Kirchhoff's Formula to Radiation From Moving Surfaces," *Journal of Sound and Vibration*, Vol. 123, No. 3, 1988, pp. 451–460.

[18] Lockard, D. P., "An Efficient, Two-Dimensional Implementation of the Ffowcs Williams and Hawkings Equation," *Journal of Sound and Vibration*, Vol. 229, No. 4, 2000, pp. 897–911.

[19] Lee, Y. W., and Lee, D. J., "Derivation and Implementation of the Boundary Integral Formula for the Convective Wave Equation in Time-Domain," *Journal of the Acoustical Society of America*, Vol. 136, No. 6, 2014, pp. 2959–2967.

[20] Morse, P. M., and Ingard, K. U., *Theoretical Acoustics*, 1st ed., Princeton University Press, New Jersey, USA, 1986.

[21] Meyers, M. K., and Hausmann, J. S., "On the Application of the Kirchhoff Formula for Moving Surfaces," *Journal of Sound and Vibration*, Vol. 139, No. 1, 1990, pp. 174–178.

[22] Meyers, M. K., and Hausmann, J. S., "Computation of Acoustic Scattering from a Moving Rigid Surface," *Journal of the Acoustical Society of America*, Vol. 91, No. 5, 1990, pp. 174–178.

[23] Kierkegaard, A., Boij, S., and Efraimsson, G., "A Frequency-Domain Linearized Navier-Stokes Equations Approach to Acoustic Propagation in Flow Ducts with Sharp Edges," *Journal of the Acoustical Society of America*, Vol. 142, No. 4, 2010, pp. 710–719.

[24] Iob, A., Arina, R., and Schipani, C., "Frequency-Domain Linearized Euler Model for Turbomachinery Noise Radiation Through Engine Exhaust," *American Institute of Aeronautics and Astronautics Journal*, Vol. 48, No. 4, 2010, pp. 848–858.

[25] Tam, C. K. W., and Auriault, L., "Time-Domain Impedance Boundary Conditions for Computational Aeroacoustics," *American Institute of Aeronautics and Astronautics Journal*, Vol. 34, No. 5, 1996, pp. 917–923.

[26] Birgisson, B., Siebrits, E., and Peirce, A. P., "Elastodynamic Direct Boundary Element Methods with Enhanced Numerical Stability Properties," *International Journal for Numerical Methods in Engineering*, Vol. 46, No. 6, 1999, pp. 871–888.

[27] Davies, P. J., "A Stability Analysis of a Time Marching Scheme for the General Surface Electric Field Integral Equation," *Applied Numerical Mathematics*, Vol. 27, No. 1, 1998, pp. 33–57.

[28] Davies, P. J., and Duncan, D. B., "Averaging Technique for Time-Marching Schemes for Retarded Potential Integral Equations," *Applied Numerical Mathematics*, Vol. 23, No. 3, 1997, pp. 291–310.

[29] Dodson, S. J., Walker, S. P., and Bluck, M. J., "Implicitness and Stability of Time-Domain Integral Equation Scattering Analysis," *Applied Computational Electromagnetics Society Journal*, Vol. 13, 1998, pp. 291—301.

[30] Hu, J. L., and Chan, C. H., "Improved Temporal Basis Function for Time-Domain Electric Field Integral Equation Method Acceleration for 3-D Electromagnetic Analysis," *Electronics Letters*, Vol. 35, No. 11, 1999, pp. 883–885.

[31] Jiang, G. X., Zhu, H. B., Ji, G. Q., and Cao, W., "Improved Stable Scheme for the Time-Domain Integral Equation Method," *IEEE Microwave and Wireless Components Letters*, Vol. 17, No. 1, 2007, pp. 1–3.

[32] Rynne, B. P., and Smith, P. D., "Stability of Time Marching Algorithms for the Electric Field Integral Equation," *Journal of Electromagnetic Waves and Applications*, Vol. 4, No. 12, 1990, pp. 1181–1205.

[33] Smith, P. D., "Instabilities in Time Marching Methods for Scattering: Cause and Rectification," *Electromagnetics*, Vol. 10, No. 4, 1990, pp. 439–451.

[34] Burton, A. J., and Miller, G. F., "The Application of Integral Equation Methods to the Numerical Solution of Some Exterior Boundary Problems," *Proceedings of the Royal Society of London*, Vol. 323, No. 1553, 1971, pp. 201–210.

[35] Meyer, W. L., Bell, W. A., Zinn, B. T., and Stallybrass, M. P., "Boundary Integral Solutions of Three-Dimensional Acoustic Radiation Problems," *Journal of Sound and Vibration*, Vol. 59, No. 2, 1978, pp. 245–262.

[36] Hu, F. Q., "On Hybrid Temporal Basis Functions for Stable Numerical Solution of Time Domain Boundary Integral Equations," *Advances in Aerodynamics*, Vol. 1, No. 9, 2019, pp. 1–18.

[37] Hu, F. Q., Pizzo, M. E., and Nark, D. M., "On the Assessment of Acoustic Scattering and Shielding by Time-Domain Boundary Integral Equation Solutions," *22nd AIAA/CEAS Aeroacoustics Conference*, American Institute of Aeronautics and Astronautics, AIAA paper 2016–2779, 2016.

[38] Hu, F. Q., Pizzo, M. E., and Nark, D. M., "A New Formulation of Time-Domain Boundary Integral Equation for Acoustic Wave Scattering in the Presence of a Uniform Mean Flow," *23rd AIAA/CEAS Aeroacoustics Conference*, American Institute of Aeronautics and Astronautics, AIAA paper 2017–3510, 2017.

[39] Zheng, C.-J., Chen, H.-B., Gao, H.-F., and Du, L., "Is the Burton-Miller Formulation Really Free of Fictitious Eigenfrequencies?" *Engineering Analysis with Boundary Elements*, Vol. 59, No. 1, 2015, pp. 43–51.

[40] Nayfeh, A. H., Kaiser, J. E., and Telionis, D. P., "Acoustics of Aircraft Engine-Duct Systems," *American Institute of Aeronautics and Astronautics Journal*, Vol. 13, No. 3, 1975, pp. 130–153.

[41] Li, X. Y., Li, X. D., and Tam, C. K. W., "Improved Multipole Broadband and Time-Domain Impedance Boundary Condition," *American Institute of Aeronautics and Astronautics Journal*, Vol. 50, No. 2, 2012, pp. 980–984.

[42] Rienstra, S. W., "Impedance Models in Time-Domain Including the Extended Helmholtz Resonator Model," American Institute of Aeronautics and Astronautics, AIAA paper 2006–2686, 2006.

[43] Spillere, A. M. N., Medeiros, A. A., and Cordiolo, J. S., "An Improved Impedance Education Technique Based on Impedance Models and the Mode Matching Method," *Applied Acoustics*, Vol. 129, No. 2018, 2017, pp. 322–334.

[44] Reymen, Y., Baelmans, M., and Desmet, W., "Efficient Implementation of Tam and Auriault's Time-Domain Impedance Boundary Condition," *American Institute of Aeronautics and Astronautics Journal*, Vol. 24, No. 9, 2008, pp. 2368–2376.

[45] Zhang, Q., and Bodony, D. J., "Numerical Simulation of Two-Dimensional Acoustic Liners with High-Speed Grazing Flow," *American Institute of Aeronautics and Astronautics Journal*, Vol. 49, No. 2, 2011, pp. 365–382.

[46] Allam, S., and Abom, M., "Experimental Characterization of Acoustic Liners with Extended Reaction," *14th AIAA/CEAS Aeroacoustics Conference*, American Institute of Aeronautics and Astronautics, AIAA paper 2008–3074, 2008.

[47] Tam, C. K. W., *Computational Aeroacoustics: A Wave Number Approach*, 1st ed., Cambridge University Press, New York, USA, 2012.

[48] Davies, P. J., and Duncan, D. B., "Stability and Convergence of Collocation Schemes for Retarded Potential Integral Equations," *Society for Industrial and Applied Mathematics Journal on Numerical Analysis*, Vol. 42, No. 3, 2004, pp. 1167–1188.

[49] Wang, H., Henwood, D. J., Harris, P. J., and Chakrabarti, R., "Concerning the Cause of Instability in Time-Stepping Boundary Element Methods Applied to the Exterior Acoustic Problem," *Journal of Sound and Vibration*, Vol. 305, No. 1, 2007, pp. 289–297.

[50] Jang, H.-W., and Ih, J.-G., "Stabilization of Time Domain Acoustic Boundary Element Method for the Exterior Problem Avoiding the Nonuniqueness," *Journal of the Acoustical Society of America*, Vol. 133, No. 3, 2013, pp. 1237–1244.

[51] Pizzo, M. E., Hu, F. Q., and Nark, D. M., "Simulation of Sound Absorption by Scattering Bodies Treated with Acoustic Liners Using a Time-Domain Boundary Element Method," *24th AIAA/CEAS Aeroacoustics Conference*, American Institute of Aeronautics and Astronautics, AIAA paper 2018–3456, 2018.

[52] Dragna, D., Pineau, P., and Blanc-Benon, P., "A Generalized Recursive Convolution Method for Time-Domain Propagation in Porous Media," *Journal of the Acoustical Society of America*, Vol. 138, No. 2, 2015, pp. 1030–1042.

[53] Troian, R., Dragna, D., Bailly, C., and Galland, M. A., "Broadband Liner Impedance Eduction for Multimodal Acoustic Propagation in the Presence of a Mean Flow," *Journal of Sound and Vibration*, Vol. 392, No. 1, 2017, pp. 200–216.

[54] Hu, F. Q., Pizzo, M. E., and Nark, D. M., "On a Time-Domain Boundary Integral Equation Formulation for Acoustic Scattering by Rigid Bodies in Uniform Mean Flow," *Journal of the Acoustical Society of America*, Vol. 142, No. 6, 2017, pp. 3624–3636.

[55] Randall, R. H., *An Introduction to Acoustics*, 1st ed., Addison-Wesley Press, Inc., Massachusetts, USA, 1951.

[56] Pierce, A. D., *Acoustics: An Introduction to Its Physical Principles and Applications*, 3rd ed., Acoustical Society of America, New York, USA, 1994.

[57] Butcher, J. C., *Numerical Methods for Ordinary Differential Equations*, 3rd ed., John Wiley and Sons, Ltd., West Sussex, United Kingdom, 2016.

[58] Jones, M. G., "Liner Technology Facility, NASA Langley Research Center," `stab.larc.nasa.gov/facilities/liner-technology-facility`, 2020. Accessed 22 Feb. 2020, Last Modified 30 Apr. 2014.

[59] Nark, D. M., and Jones, M. G., "Assessment of Axial Wave Number and Mean Flow Uncertainty on Acoustic Liner Impedance Eduction," American Institute of Aeronautics and Astronautics, AIAA paper 2018–3444, 2018.